frontiers | Frontiers in Marine Science

TYPE Original Research
PUBLISHED 18 November 2024
DOI 10.3389/fmars.2024.1481299

OPEN ACCESS

EDITED BY
Hajime Kayanne,
The University of Tokyo, Japan

REVIEWED BY
Jose Luis Antinao,
Indiana University, United States
Santosh Kumar Rai,
Wadia Institute of Himalayan Geology, India

*CORRESPONDENCE
Pankaj Khanna
pankaj.khanna@iitgn.ac.in

RECEIVED 15 August 2024
ACCEPTED 07 October 2024
PUBLISHED 18 November 2024

CITATION
Misra SK, Menon S, Sahoo R, Mannu U and Khanna P (2024) Holocene fringing reef along southern Andaman and Swaraj Dweep shoreline. *Front. Mar. Sci.* 11:1481299. doi: 10.3389/fmars.2024.1481299

Holocene fringing reef along southern Andaman and Swaraj Dweep shoreline

Saikat Kumar Misra[1], Shradha Menon[1], Ramendra Sahoo[2], Utsav Mannu[1] and Pankaj Khanna[1]*

[1]REEFS Lab, Department of Earth Sciences, Indian Institute of Technology Gandhinagar, Palaj, Gandhinagar, India, [2]CSIR-National Geophysical Research Institute, Hyderabad, India

The Andaman and Nicobar Islands are rimmed by discontinuous fringing reef that is in general wider on western margin vs the eastern margin. This study characterizes the facies updip from the modern fringing reefs to the present shoreline of south Andaman and Swaraj Dweep, and describes in detail the coral terraces/carpets within and above the inter-tidal zone representing the Holocene Fringing reef. Field studies, satellite, and drone datasets have been utilized to map different facies, that include: coralgal boundstone, biodetrital-grainstone, beachrock, and coralgal rudstone. Multiple exposed microatolls as well as coral terraces (coral carpets) of *Acropora* and *Porites* (dated 8.7-8.4 ka BP) have been identified within the intertidal zone (Radhanagar Beach, Swaraj Dweep) indicating that Holocene fringing reef have down-stepped offshore to the current location of modern fringing reefs owing to either tectonics or eustasy. The eustatic sea-level fluctuations are relatively well established for the Holocene and we compute the tectonic uplift rates utilizing the stream-power-incision and linear-inversion model. A tectonic uplift rate of ~ 0.05 mm/yr (for Swaraj Dweep) during the past 100 ka is estimated, while taking into account a wide range of erodibility indexes and response time intervals. It is identified that the computed uplift rate is an amalgamation of the coseismic deformation along with the interseismic and aseismic surface deformation. Thus, not all exposed coral terraces/microatolls are exposed due to coseismic deformation (for example uplift in parts of Andaman due to earthquake in 2004). The average long-term uplift rates are a magnitude lower than the eustatic sea-level fall rates during Holocene, thus, we suggest that most of the Holocene fringing reefs are exposed due to eustatic sea-level fall and down-stepped to the current location of the modern fringing reefs. This would entail that the eustatic sea-level change rates would play a significant role in determining future of the modern fringing reef (catch-up vs keep up vs give up), and the coastal morphology of south Andaman and Swaraj Dweep, with implications for coastal inundation and stability in the scenario of climate change.

KEYWORDS

coral reef, terraces, Indian Ocean, sea-level, shallow marine carbonates

Introduction

Reefs that are close to shore, often attached, usually thin veer of seaward thickening carbonate sediments over non-reefal topography are defined as fringing reefs (Steers et al., 1977). At present, the majority of the Andaman and Nicobar Islands (off the coast of the Indian subcontinent), have discontinuous fringing reefs along the eastern and western margins (Rodolfo, 1969; Gibson et al., 2007). The growth of the fringing reefs are greatly influenced by sea-level fluctuations and tectonics (Kennedy and Woodroffe, 2002; Droxler and Jorry, 2013), as well as hydrodynamics near the coastal margin and the geographic location (Freeman et al., 2012; Wall et al., 2012; Lenihan et al., 2015). The reef ecology and morphology can be used to gain insights into the sea-level fluctuations, which in turn could be used to derive uplift/subsidence rates in tectonically active regions (Schlager, 2005; Dorobek, 2008; Meltzner et al., 2010; Woodroffe and Webster, 2014; Khanna et al., 2017). Moreover, variations in facies can serve as analogues to understand the evolution of these systems in response to variations in the environment (sea-level and climate; Kennedy and Woodroffe, 2002; Yamano et al., 2003; Cabioch et al., 2008).

Due to the lack of long-term ecological datasets, it is difficult to predict how reefs might respond to ongoing climate warming (Greenstein and Pandolfi, 2008); however, fossil reefs, especially the Holocene reefs, have recorded the past changes, by either modifying their assemblage (Montaggioni, 2005), or by backstepping or downstepping (Steers et al., 1977; Davies and Hopley, 1983; Neumann, 1985) and/or by drowning (Buddemeier and Hopley, 1988). The fringing reefs occur in conditions that are considered already marginal (Perry, 2003); thus, it is even more important to understand their morphologies, assemblages, and the major factors influencing their growth as they are natural barriers to coastal erosion for several islands. Coastal areas and low-lying regions with less than 2 m elevation host about 11% of the global population and will thus be adversely affected by the rise in global mean sea-level in the near future (Neumann et al., 2015; Magnan et al., 2019). It is, therefore, critical to understand how fringing reefs respond to sea-level fluctuations induced by tectonics, eustasy and global isostatic adjustment (GIA), not just on a shorter time scale but also on longer time scales (Khan et al., 2019).

The Andaman Archipelago is situated within an accretionary wedge system and is tectonically active, resulting from the subduction of the Indian plate beneath the Burmese plate (Curray et al., 1979; Dasgupta et al., 2003; Ghosh et al., 2017). The 2004 earthquake caused subsidence in the southeastern part of Andaman, while uplift occurred in the northwestern part (Meltzner et al., 2006; Kayanne et al., 2007), which led to a rapid change in coastal morphology and exposure of some modern reef terraces. Some coral samples from Radhanagar beach (Andaman Islands - Swaraj Dweep), dating back approximately 8.7-8.4 ka (Awasthi et al., 2013), were also found in the upper intertidal zone representing a late-mid-Holocene age. Thus, the objective of this study is to investigate the exposed discontinuous fringing reef and adjacent facies along south Andaman and Swaraj Dweep to discern the evolution of the shallow marine carbonates in the Andaman Islands in response to tectonics and sea-level change. This would entail –

1. Mapping the shoreline throughout south Andaman and Swaraj Dweep and recognizing the prominent facies both through satellite imagery and field investigations.
2. Modeling of river profiles using stream power laws and linear inversion models to understand the relative uplift rates upto 1 Ma.

This study will allow us to understand the processes that contributed to the evolution and ultimate demise of the Holocene fringing reefs of south Andaman and Swaraj Dweep.

Regional settings

The Andaman Islands are located between 6°N to 14°N and 92°E to 94°E, off the eastern margin of India (in the Bay of Bengal). The exposed rocks in the group of islands have been dated from Cretaceous to Recent, with the stratigraphy as follows - the Cretaceous Ophiolite Group, Eocene Mithakali Group, Andaman Flysch Group from the Eocene to Upper Oligocene and the Young Archipelago Group from the Lower Miocene (Bandopadhyay and Carter, 2017). The stratigraphic relationship is complex due to obduction. Modern sediments, including the shallow marine carbonate systems, overlie the rock substrate (Ghosh et al., 2017). The Ophiolite Group is composed of both lower crustal cumulates-depleted mantle harzburgite, dunite, gabbros, peridotites and upper crustal sheeted dikes, pillow lavas, and marine pelagic sediments (Ray et al., 1988; Bandyopadhyay et al., 2020). The Mithakali Group comprises immature gravels, pebbly to fine-grained pyroclastic sandstones, coarse- to fine-grained sandstones, and a few small thin layers of mudstones (Allen et al., 2008). The Andaman Flysch, which consists of siliciclastic sediments, was originally deposited as turbidites within a submarine fan system (Chakraborty and Pal, 2001). The Archipelago group of rocks is the uppermost stratigraphic unit of the Tertiary period, primarily composed of limestones, mudstones, chalk and shales, which have been deposited in shallow to deep marine environments (Bandopadhyay and Carter, 2017). The majority of these rocks can be observed in Richie's Archipelago, a series of small island chains located in the east of south Andaman (e.g., in Swaraj Dweep; Bandopadhyay and Carter, 2017; Desai, 2021). Pleistocene rocks of the Neil Limestone Member are visible in Shaheed Dweep (Neil) and have biodetrital carbonate components consisting of corals and algae, as well as foraminifera and polycrystalline quartz grains (Chakraborty et al., 2017). Overlying this member unconformably are recent deposits of shell limestone that include boulders, pebbles, rubbly limestone, and beach sands (Sharma and Srinivasan, 2007). The modern shallow marine carbonate systems include coral reefs, patch reefs, lagoons, and tidal flats (Menier et al., 2014). The reefs are present extensively at depths ranging from 1-20 meters and are dominated by different species of finger and massive corals such as *Acropora, Porites, Montipora, Favia*, etc. (Wafar, 1986).

Methodology

Field and lab study

Field work was conducted in south Andaman and Swaraj Dweep (Figure 1; Table 1) in May 2023 (10 days) and Feb 2024 (10 days). Systematic coastal mapping was conducted along twelve beaches (Table 1; Nine – south Andaman, three – Swaraj Dweep). Garmin GPS Montanna 680 was utilized to mark and map different morphological features along the different beaches (terraces, microatolls, rocky shoreline/grainy shoreline). Hand samples (loose/unconsolidated sediments) and cores (consolidated limestone) were collected from the beaches to further identify and map the coastal facies within the intertidal zone and shallow marine environments up to the fringing reefs.

20 g sample from the hand samples collected in field were dried and wet sieved and the mass loss after drying was calculated. Further, different sieves with varying mesh sizes: >2 mm, >0.500 mm, >0.250 mm, >0.125 mm, and >0.063 mm were used to separate the sample into different size fractions. Additionally, some thin-sections were prepared by Continental Labs (Thin section preparation lab in Uttar Pradesh, India), and studied under a Leica DM750 polarizing microscope. In this study, we focused on thin sections containing grain sizes larger than 0.500 mm diameter (to identify carbonate components). Sediment/rock composition has been classified based on texture (based on the matrix and grain percentage; Dunham, 1962). Here, sediments from the shoreline were classified depending on their mud content: –<10% grainstone, 10 – 26% packstone to grainstone, 26 – 42% packstone, 42 – 58% wackestone to packstone, 58 – 74% wackestone, 74 – 90% mudstone to wackestone and >90% mudstone (Petrovic et al., 2022; Menon et al., 2024). Further, *in situ* coralgal massive structures were categorized according to (Embry and Klovan, 1971), providing a more precise facies classification of all allochthonous and autochthonous component. Facies map for the south Andaman and Swaraj Dweep were created using QGIS 3.34.6 LTR©.

Drone data acquisition and processing

This study utilized a custom X8 configuration multi-rotor drone (Bajrang Drone Series), referred to as a UAV from here-on, equipped with 20 MPX camera to collect visible RGB imagery over the coastal area and shallow (< 1 m) water zones within south Andaman and Swaraj Dweep. The UAV was equipped with a gimbal to keep the camera in a horizontal position at all times, thus reducing the data acquisition errors.

Five UAV surveys were conducted to collect >1500 digital photographs covering five areas, that are Badabalu Beach and Burmanallah in south Andaman (Loc. 4 and 7, Table 1), and Radhanagar, Kalapathar, and Govindnagar Beach in Swaraj Dweep (Loc. 10,11, and 12 – Table 1). The UAV was flown at an

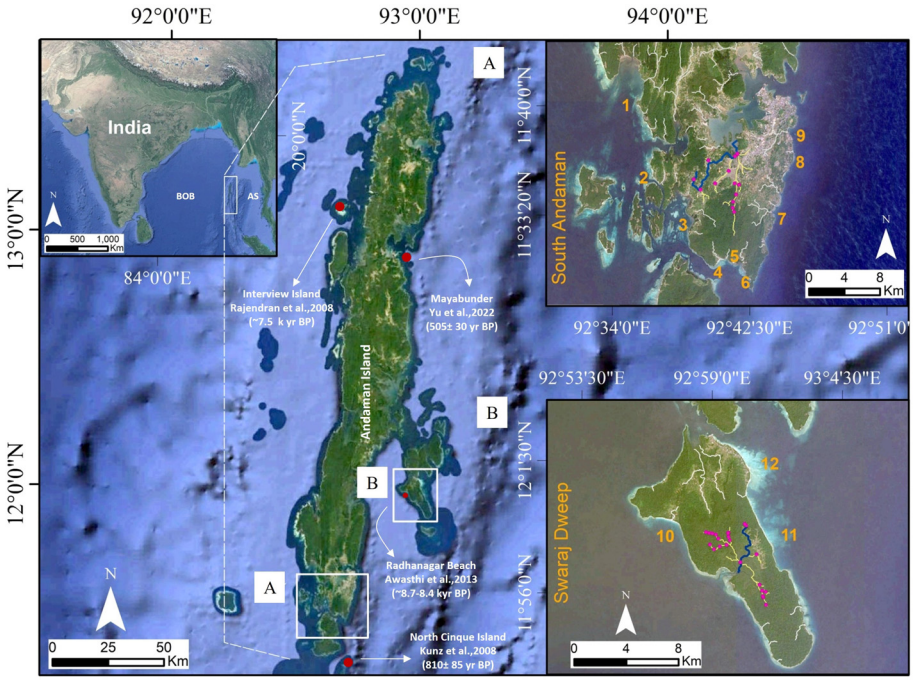

FIGURE 1
Location of Andaman Island and the Study Areas: **(A)** south Andaman, **(B)** Swaraj Dweep. The different beaches within the studied areas are numbered as follows: 1) Khurmadera, 2) Wandoor, 3) Manjeri, 4) Badabalu, 5) Chotabalu, 6) Chidiyatapu, 7) Burmanallah, 8) Brichgunj, 9) Corbyn's Cove, 10) Radhanagar, 11) Kalapathar, and 12) Govindnagar. Rivers within the studied areas are also shown. The largest channel in the area is colored in yellow, and the trunk stream that is used for river profile inversion, is colored in blue. Pink dots indicate the knick points within river (The river profiles, trunk stream and knick points are derived using the topotoolbox developed by Schwanghart and Scherler, 2014). Additionally locations of dated fossil corals from previous literature have been marked.

TABLE 1 List of studied locations along south Andaman and Swaraj Dweep.

Location names	Latitude	Longitude	Locations in Figure 1
Khurmadera Beach	11° 40.023'N	92° 35.584'E	1
Wandoor Beach	11° 35.798'N	92° 36.487'E	2
Manjery Beach	11° 32.270'N	92° 38.666'E	3
Badabalu Beach	11° 30.599'N	92° 40.627'E	4
Chotabalu Beach	11°30.486'N	92°41.46'E	5
Chidiyatapu Beach	11° 30.034'N	92° 42.114'E	6
Burmanallah Beach	11° 33.273'N	92° 43.870'E	7
Brichgunj Beach	11° 36.926'N	92° 45.173'E	8
Corbyn's Cove Beach	11° 38.681'N	92° 44.946'E	9
Radhanagar Beach (Swaraj Dweep)	11° 59.062'N	92° 57.034'E	10
Kalapathar Beach (Swaraj Dweep)	11° 59.936'N	93° 0.480'E	11
Govindnagar Beach (Swaraj Dweep)	12° 0.946'N	93° 0.602'E	12

above-ground height of ~80 m over the area, with the camera in nadir orientation with a 90% overlap.

Agisoft Metashape Professional 1.8.4 was used to reconstruct dense 3-D models resulting in five photogrammetric digital outcrop models (e.g., Khanna et al., 2020). These were meshed and textured (by back-projecting the original image data) and converted to an orthomosaic to interpret spatial distribution of sediment facies across various sections of the shoreline the facies zone boundaries.

Stream Power Incision Model (SPIM) and linear inversion of river profiles

River profiles are a good proxy of base-level change and have been widely used to get an estimate of tectonic and climate history in different geographical settings (Pedersen et al., 2018; Stucky de Quay et al., 2019; Ma et al., 2020; Sonam et al., 2021; Su et al., 2022; Clementucci et al., 2023). Any change in the base level creates a potential (knick point) at the river mouth, which then propagates upstream along the river network through erosion (Howard, 1994). This process can be mathematically expressed as a mass balance

$$\frac{dz}{dt} = U - E \tag{1}$$

where, z is the river profile elevation, U is the uplift rate (assumed to be block uplift) and E is the erosion rate. The erosion rate term can be modeled as a linear advection term (stream power law), where the wave velocity (migration velocity of the knickpoints) is a product of the rock erodibility (K), upstream contributing area (A) and channel gradient/slope (S) (Flint, 1974; Whipple and Tucker, 1999).

$$E = KA^m S^n \tag{2}$$

The rock erodibility, K, is an empirical parameter in the Stream Power Incision Model (SPIM) and an integration of various physical variables affecting the resistance to erosion. The relative contribution of climate and tectonics to the erosion process is determined by the power terms m and n. Overall, the advection equation with the source term as the uplift takes the following form

$$\frac{\partial z}{\partial t} = U(x,t) - KA^m \left(\frac{\partial z}{\partial x}\right)^n \tag{3}$$

The above equation can be further linearised by taking the exponent of the slope (n) as 1. Studies generally find that linearised inversion results with $n = 1$ lead to a better fit between measured and predicted river profiles (Pritchard et al., 2009; Goren et al., 2014). The solution to the above linear advection equation ($n = 1$) is given in the following integral form

$$Z(x,t) = \int_{t-\tau_x}^{t} U[\tau^{-1}(\tau_x - t + s, s)]ds \tag{4}$$

where τ_x is the travel time of an advection wave from the river outlet (where the uplift signal is getting generated x = 0) to any point of the river profile x = x, and is mathematically represented as

$$\tau_x = \int_0^x dx/KA_x^m \tag{5}$$

In Equation 4, s is a dummy variable for the integral. $\tau^{-1}(t)$ is the inverse function of $\tau(x)$, i.e., $\tau^{-1}(\tau(x)) = x$. This inverse function maps the response time and position x, transforming the distance along the channel from the river outlet into its corresponding response time. Further, the t in the upper limit of the integral in Equation 4 becomes zero as we use the present (t=0) topography as our input data.

Here, we have assumed the uplift/base level fall to be space invariant. Then, Equation 4 simplifies to

$$Z(x,0) = \int_{-\tau_x}^{0} U[\tau^{-1}(\tau_x + s, s)]ds \tag{6}$$

The above equation, in matrix form, can be rewritten as follows

$$AU = z \tag{7}$$

where, A is the forward operator matrix and contains the response time terms for all the nodes of the river profile (Goren et al., 2014). We can use the linear least square solution of the above equation to find the U term

$$U = U_p + (A^T A + \delta^2 I)^{-1} A^T (z - AU_p)$$

where, δ is a damping factor used to account for the ill-posed and unstable nature of the problem and the solution respectively, I is the identity matrix and Up is the prior uplift rate, which gets updated through the least-square method (Goren et al., 2014). The present study utilized SRTM digital elevation models (DEM) with a 30 m resolution to assess the uplift rate in the south Andaman and Swaraj Dweep. The model's outputs facilitated the estimation of relative subsidence and uplift rates, which are factors that would have

gradually impacted the topography. The values reported in the literature were utilized to determine the model parameters (rock erodibility (K) and area exponent (*m*)) in the absence of any prior information regarding the study area. Assuming $n = 1$, the value of *m* generally ranges from 0.4 to 0.6 and is not significantly influenced by the uplift rate (Whipple and Tucker, 1999; Kirby and Whipple, 2012). A mean value of 0.5 for *m* was employed in our modeling analysis, which is reported for other geographical regions with similar lithology and climate (Montgomery and Gran, 2001). The erosion coefficient or erodibility value employed in this research was 4.75-5.25×10^{-6} yr^{-1}, which falls toward the upper end of the documented soil erodibility values in Mount Talang, West Sumatra (Afrizal and Masunaga, 2013). Similar values (of the order of 10^{-6} yr^{-1}) have been reported for comparable rock types as those found in our study, including metasedimentary or volcanic rocks (Montgomery and Gran, 2001; Yanites et al., 2017; Morales et al., 2023), and other volcanic islands (e.g., Hawaii Island; Han et al., 2014). After fixing the values for the model parameters (*m* and K), we found the maximum response time (for the channel heads in the river network) for our study area to be ~1 Myr. Hence, we discretized the river length into intervals, each of which equated to 100 Kyr for both south Andaman and Swaraj Dweep. Interestingly, the eustatic cycles exhibited a 100 Kyr interval over the past ~1 million years (Lambeck et al., 2002). Consequently, a 100 Kyr interval was selected to mitigate the influence of eustatic component when calculating long-term tectonic uplift rates. We used the QGIS Whitebox plugin (Lindsay, 2016) through QGIS for the hydrological analysis of the DEM dataset. Additional processing of the hydrological outputs as well as river profile analysis, were carried out using Python.

Results

Geomorphic and sedimentologic description of the beaches (south Andaman and Swaraj Dweep)

South Andaman

Khurmadera: This is located in the western part of south Andaman (Figures 1, 2; Table 1). Broken coral clasts (mostly branching corals) and rubbles are accumulated along the beaches and form multiple ridges. Vegetation is covering parts of the ridges. Exposed *in-situ* dead corals are also observed along the beaches in the intertidal zone dominated by massive *Porites* corals. Moreover, the beach is also composed of medium to coarse-grained unconsolidated carbonate sand. Tidal notches, 2m above the

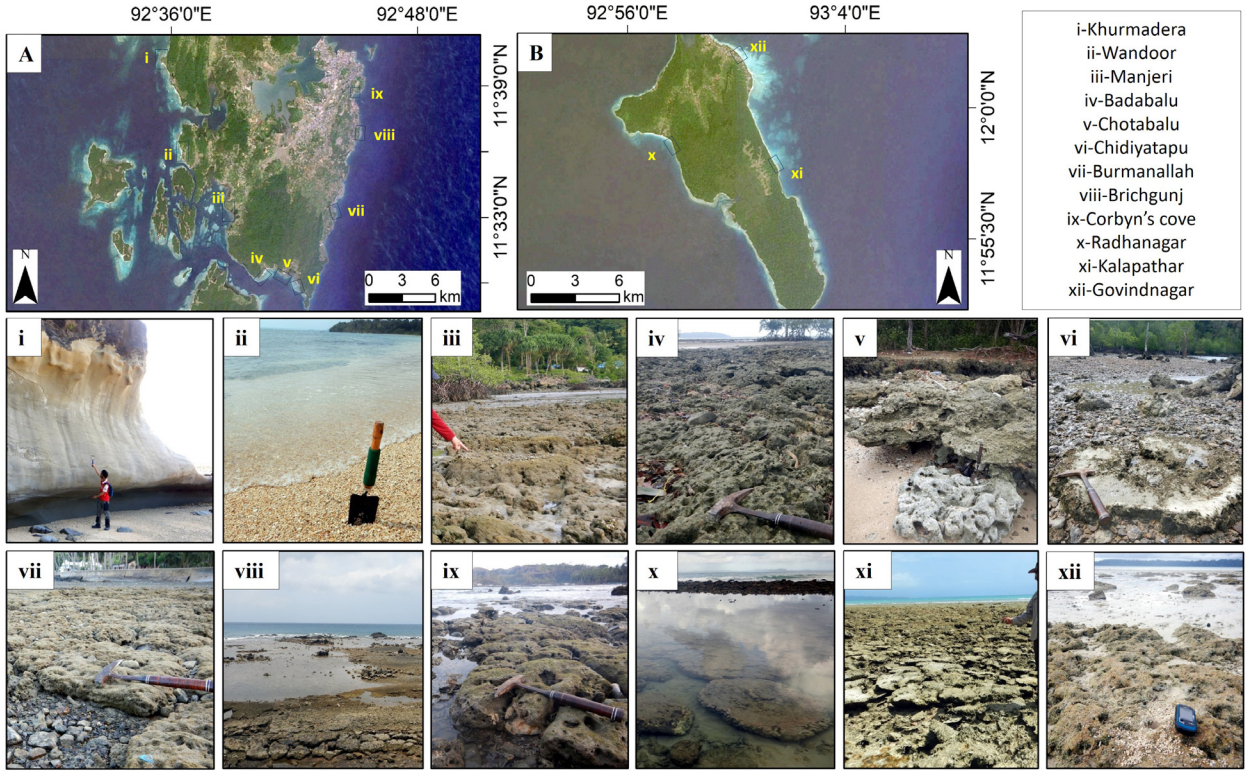

FIGURE 2
Field photographs from. **(A)** south Andaman (i–ix) **(B)** Swaraj Dweep (x–xii) islands; i) Khurmadera, featuring a ~2 m high tidal notch; ii) Wandoor, characterized by coarse carbonate sand (biodetrital grainstone); iii) Manjeri, exposed dead corals (coralgal boundstone); iv) Badabalu with exposed dead corals (coralgal boundstone); v) Chotabalu, lithified beach sediments (beachrock) overlay in-situ exposed coral; vi) Chidiyatapu, where in-situ coral is surrounded by pebbles derived from ophiolites and/or flysch; vii) Burmanallah, with exposed coral surrounded by pebbles; viii) Brichgunj, showing a layer of coralgal rudstone; ix) Corbyn's Cove, with exposed corals; x) Radhanagar featuring microatolls; xi) Kalapathar, with exposed corals; and xii) Govindnagar,exposed dead corals.

present mean tide level, have been observed along the cliffs (Figure 2i). This paleo tidal notch at higher elevation indicates either tectonic uplift or sea-level drop.

Wandoor: This beach is present in the western region of south Andaman and is located to the south of Khurmadera (Figures 1, 2; Table 1). Here, coarse carbonate sands are observed (Figure 2ii), dominated by *Halimeda* (Green algae), red algae as well other algal fragments. Some *in-situ* exposed massive corals mostly *Porites* are present in the intertidal zone.

Manjeri: The beach is also situated on the western side of south Andaman (Figures 1, 2; Table 1). Here, the intertidal zone is dominated by *in-situ* exposed corals. Here, the corals are predominantly *Porites* along with other types of corals and fragments of branching corals area also observed. (Figure 2iii). Green algae, specifically *Halimeda*, are encrusting these exposed massive corals and is also present within the intertidal zone. Silty to muddy sediments (black to grey mud) envelop the exposed reefs and are distributed throughout the intertidal zone. Siliciclastic sediments transported from inland are deposited by channels or creeks, which are subsequently dispersed along the beaches by the action of waves. Some mafic rocky layers are also exposed along the shoreline, the erosion of which has generated pebbles to cobble sized clasts.

Badabalu: The area is located in the southern part of south Andaman (Figures 1–3; Table 1). Here, the beach is dominated by coarse carbonate sands. Additionally, there are pebble to cobble sized volcanic clasts along the eastern side of the Badabalu beach. In some places, the pebbles are also present covering and/or surrounding the exposed *in-situ* corals and microatoll structure of *Porites* (Figure 2iv). The pebble to cobble sized volcanic clasts have been attributed to the erosion of the exposed mafic rock layers.

Chotabalu: This is located in the southern region of south Andaman, east of Badabalu beach (Figure 1, 2; Table 1). The Badabalu and Chotabalu sandy beaches are separated by pebble to cobble sized volcanic clasts as well as rock layers. Chotabalu beach is characterized by carbonate sands as well as exposed *in-situ* corals dominated by massive *Porites*, that are present in the intertidal to the supratidal zones. These *in-situ* dead corals are covered by lithified beach sediments at an elevation of 1 m (Figure 2v) comprising large coral clasts, clastic pebbles and numerous shells.

Chidiyatapu: This area is situated in the eastern part of Chotabalu beach (Figures 1, 2; Table 1). This part of the beach is dominated by pebbles derived from the surrounding mafic rock layers (Figure 2vi). Additionally, the shoreline here is also characterized by some *in-situ* dead corals and *Porites* microatolls.

Burmanallah: Situated on the eastern side of south Andaman (Figures 1, 2, 4; Table 1), the region is predominantly devoid of sand. The intertidal zone is characterized by *in-situ* dead massive corals dominated by *Porites*, some *Coeloseris ()?*, branching corals (Figure 2vii), as well as live corals. Within the upper intertidal zone, the dead-corals are covered by a thin layer of partially lithified carbonate sand discontinuously. Just north of Burmanallah, mafic rock layers are present along the beaches, that are overlain by dead *in-situ* corals and coral boulders. In the rocky intertidal zone, we find green algae, particularly *Halimeda*, as well as other types of brown algae. The green algae predominantly cover the exposed dead corals, while seagrass is also observed in this location.

Brichgunj: This is located in the eastern region of south Andaman (Figures 1, 2, 5; Table 1), north of Burmanallah beach. A thin layer of carbonate beach sediments is present within the upper intertidal to supratidal zone, while mafic rocky layers and pebbles characterize the lower intertidal zone. Additionally, consolidated layers containing clasts of volcanics, corals, and shells are present. This cemented rock has multiple layers sloping toward the sea and is predominantly found in the upper part of the intertidal zone (Figure 2viii).

Corbyn's Cove: This location is on the eastern margin of south Andaman (Figures 1, 2; Table 1), north of the Brichgunj area. Carbonate sediments are present in the intertidal zone. Moreover, along the northern edge of this beach, distinct patches of exposed *in-situ* dead corals prevail, primarily dominated by *Porites* and

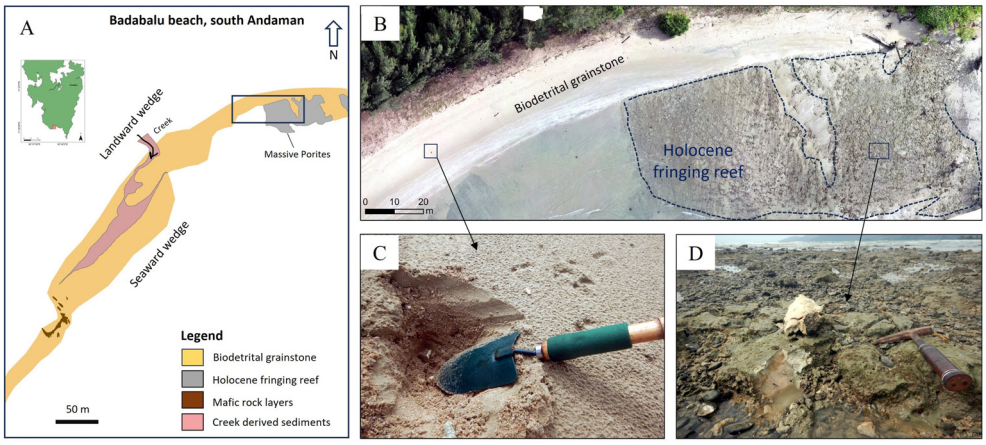

FIGURE 3
(A) Digital map of the Badabalu beach, one creek is also depositing sediments along the beach; The black rectangle depicts the region of focus in the drone imagery **(B)** Drone imagery of the area representating various coastal facies including Holocene fringing reef. **(C)** The image includes biodetrital grainstone facies and **(D)** coralgal boundstone facies.

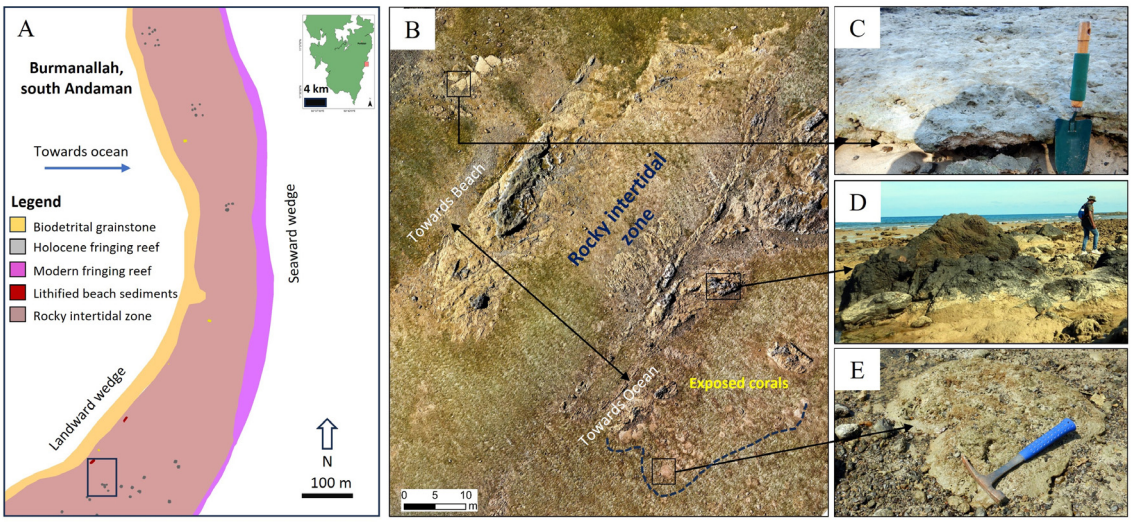

FIGURE 4
(A) Digital map of the Bumanallah section, Fossilized corals are exposed above the rocky intertidal zone; The black rectangle depicts the region of focus in the drone imagery **(B)** Drone imagery of Burmanallah beach representing various coastal facies. **(C)** beachrock **(D)** some mafic rock layers, over which **(E)** and coralgal boundstone facies are exposed.

Coeloseris()?. These corals overlay rock layers (refer to Figure 2ix). Additionally, a canal transports siliciclastic sediments from the hinterlands to the beach.

Swaraj Dweep

Radhanagar beach: This predominantly carbonate sand (coarse-grained) beach is on the western side of the Swaraj Dweep (Figures 1, 2, 6; Table 1). The northern as well as the southern margins of the Radhanagar beach are characterized by flysch/limestone rock layers. The intertidal zone adjacent to southern margin has exposed *in-situ* dead corals mostly massive *Porites* (Figure 2x). Some encrusting corals are also found approximately 2 meters above the current sea-level. These corals established above the older silty sedimentary rock layers (flysch). The intertidal-subtidal zone of this area is constituted by microatolls.

Kalapathar beach: This beach is on the eastern side of Swaraj Dweep (Figures 1, 2, 7; Table 1) and is dominated by carbonate sand. Along the shoreline, as we move south, exposed *in-situ* corals are present distributed along a wide stretch (10-100 m) in the intertidal zone (Figure 2xi). It is dominated by dead massive and platy corals. The intertidal zone also has exposed older sedimentary rock layers. These older silty sedimentary rock layers are overlain or

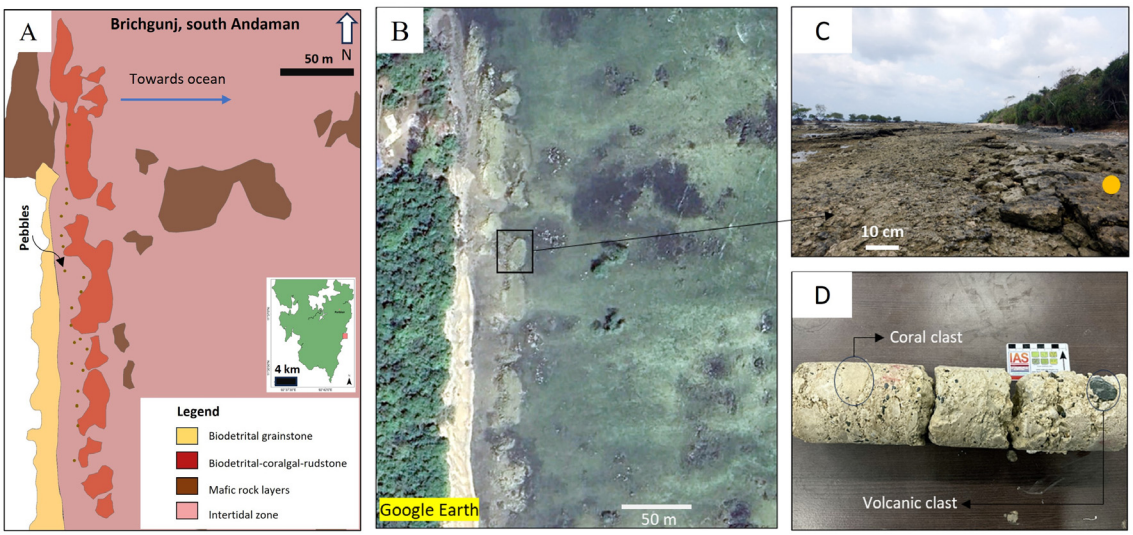

FIGURE 5
(A) Digital map of the Brichgunj area **(B)** Google Earth imagery of the same area, showing rudstone facies along Brichgunj Beach **(C)**The image depicts the rudstone layers inclining toward the ocean **(D)**, and a drilled core from the apex of the Rudstone layer, revealing numerous coral fragments and volcanic clasts.

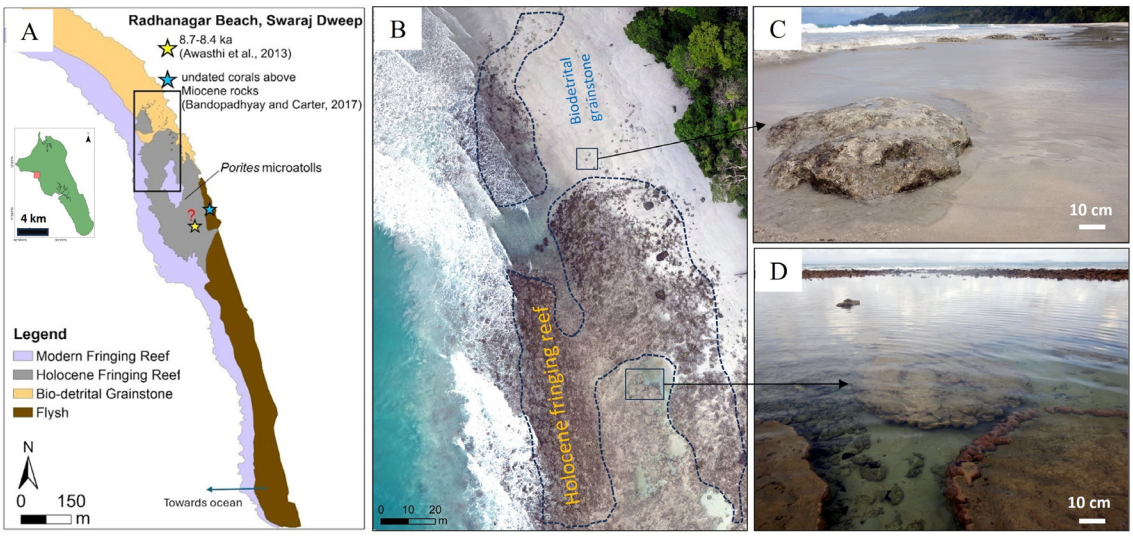

FIGURE 6
(A) Digital map depicting the facies of Radhanagr beach. The arrow depicts the seaward edge. The stars indicate the possible location of the dated samples (references in figure). The black rectangle depicts the region of focus in the drone imagery shown in **(B)**. **(B)** Drone imagery of Radhanagar Beach representing various coastal facies-dominantly Holocene fringing reef. **(C)** The image includes isolated exposed coral covered by biodetrital grainstone **(D)** microatolls in intertidal zone (coralgal boundstone).

surrounded by corals. Further, the corals are overlain by cemented coarse-grain sediment layers. The northern part of the Kalapathar beach also has some exposed corals.

Govindnagar: Located north of Kalapathar beach, in the eastern part of Swaraj Dweep (Figures 1, 2, 8), it is characterized by carbonate sand. Massive exposed dead corals are also present in the upper intertidal zone (Figure 2xii). In this location, fossilized corals are primarily composed of the *Porites*, alongside other massive and encrusting coral types are also observed. The lower intertidal zone is marked by fine grained carbonates and seagrass. Additionally, abundant mangroves are present along the shoreline.

Facies

The shoreline along the south Andaman and Swaraj Dweep can be categorized as either rocky or sandy (Figures 3–9). The intertidal zone adjacent to the rocky shorelines (vestiges of ophiolites, lower

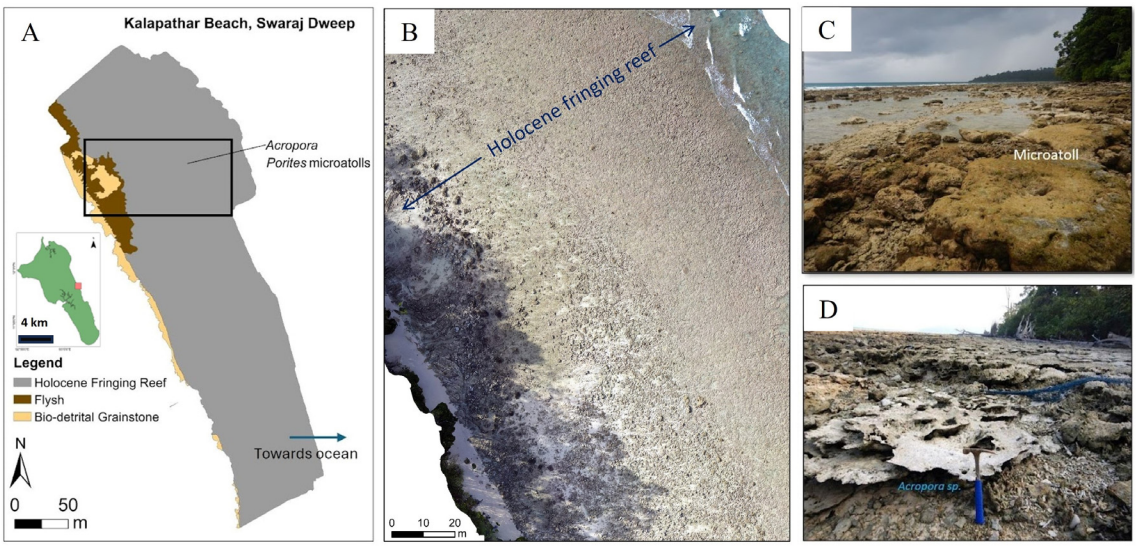

FIGURE 7
(A) Map of Kalapathar repressing the dominant facies. The arrow depicts the seaward edge. The black rectangle corresponds to the region of interest in the drone imagery in **(B)**. **(B)** Drone imagery of Kalapthar Beach representing various coastal facies; i.e., coralgal boundstone (both **C, D**). **(C)** microatoll of *Porites* **(D)** *Acropora* sp.

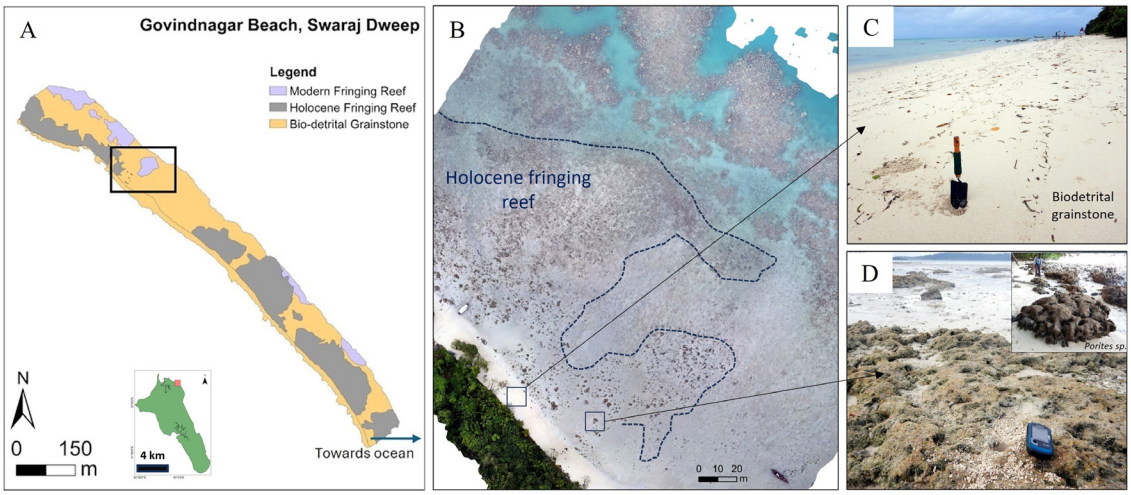

FIGURE 8
(A) Map of Govindnagar beach with the predominant facies depicted. The arrow depicts the seaward edge. The black rectangle indicates the region of focus and the drone imagery of the particular region is shown in **(B)**. **(C)** biodetrital grainstone **(D)** coralgal boundstone facies, *Porites* sp are primarily dominant.

mantle rocks or flysch) are characterized by reworked broken clasts. The rocky shorelines are predominant in Chotabalu, Chidiyatapu, Brichgunj and Burmanallah (Figures 4, 5, 9). The sandy shorelines have either unconsolidated carbonate sands, coral terraces, consolidated facies or silty-to-muddy mixed carbonate-siliciclastic in the intertidal zone. Adjacent to the intertidal facies are the fringing reefs. A detailed description of the facies (Figure 9) is provided in the section below.

Biodetrital grainstone

It is mainly composed of carbonate sediments with grain size varying from gravel-sized (>2mm) to sand (0.5mm – 0.063mm). Coral clasts, molluscs, algae and microfossils form the major components (Figure 10). Generally, the grain size decreases from the upper to lower intertidal zone. The biodetrital grainstone facies is a major component, particularly in Khurmadera, Wandoor, Badabalu (Figure 3B), Chotabalu and Corbyn's Cove in south

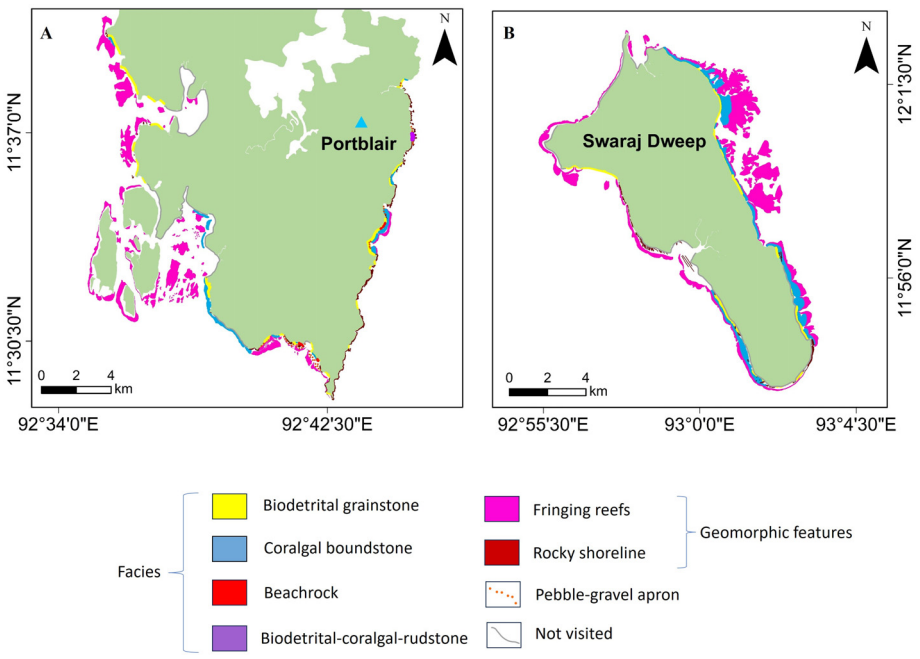

FIGURE 9
Facies distribution map of the coastal areas in south Andaman **(A)** and Swaraj Dweep **(B)**. The map depicts the various facies (see legend), primarily the modern day fringing reef and the associated facies. Rocky coastlines have also been added to indicate regions wherein ophiolites/mafic rocks/ flysch are observed in abundance.

Andaman, and Radhanagar (Figure 6B) and Govindnagar (Figure 8B) beaches in Swaraj Dweep.

Coralgal boundstone

Coral and some coralline algae make the framework of coralgal boundstone facies. It is usually located within the intertidal zone and in some cases the supra-tidal zone as extensive coral terraces/carpets that are a several hundred meter long and up to few 10's to 100's of meters wide (dimensions vary across various beaches; Figure 7A). This facies has been identified along the beaches of south Andaman beaches (Badabalu, Chotabalu) and Swaraj Dweep (Radhanagar, Kalapathar and Govindnagar) (Figures 6B, 7B, 8B).

Beachrock

Lithified beach sediments are observed on the southern, western and eastern coast of south Andaman, such as in Chotabalu, Chidiyatapu, Wandoor and Burmanallah. These cemented sediments are mostly present unconformably over exposed coralgal boundstone facies or mafic rock layers. These are mostly silty to sandy in nature, dominated by corals, microfossils and mollusc clasts and are present along the upper intertidal to supratidal zones in discrete patches.

Biodetrital-Coralgal-Rudstone

It is a clast-supported rock facies, present in the sub to supratidal area of the Chotabalu and Brichgunj area (Figures 5B, C), with varying elevations (present-day sea-level in Brichgunj and within 2m of low tide level in Chotabalu). The clasts are >2mm sized (gravel-sized), constituted by coral fragments (not *in-situ*), volcanic clasts and bivalves (Figure 5C). These beds dip toward the ocean and exhibit evidence of modern bioerosion in the form of borings made by worms, crabs and/other microborers.

Modeling from DEM analysis

We modeled a 1D river profile inversion, for calculating base-level fall vs time, using three K values (4.75×10^{-6}-,5×10^{-6} yr^{-1}, 5.75×10^{-6}-,5×10^{-6} yr^{-1}, and 5.25×10^{-6} $yr^{-1)}$ with a tolerance of ± 5% (for K=5×10^{-6} yr^{-1}; Figure 11). Further, we only considered the trunk streams of the river network for inverse modeling. We considered a cutoff flow length greater than 5 km as colluvial processes (such as debris flow) dominate shorter rivers (Wohl, 2020). The west-flowing rivers in south Andaman are shorter than the cutoff flow length. Hence, we considered only the east-flowing rivers from south Andaman for modeling. However, for Swaraj Dweep, we took the trunk streams that flow from the northeast side to the southwest side of the island and have a cutoff length greater than 5 km.

Modeling studies reveal an average base-level fall rate of 0.13(± 0.001) mm/yr and 0.05(± 0.002) mm/yr for south Andaman and Swaraj Dweep respectively (Figures 11, 12). Nevertheless, there are significant variations in the base-level fall rate. For instance, the average base-level fall rate for the south Andaman varies 0.2 mm/yr (before ~800 Kyr) to 0.13 mm/yr (between 400 and 800 Kyr) to a relatively low rate of 0.06 mm/yr (from ~400 Kyr to present). A

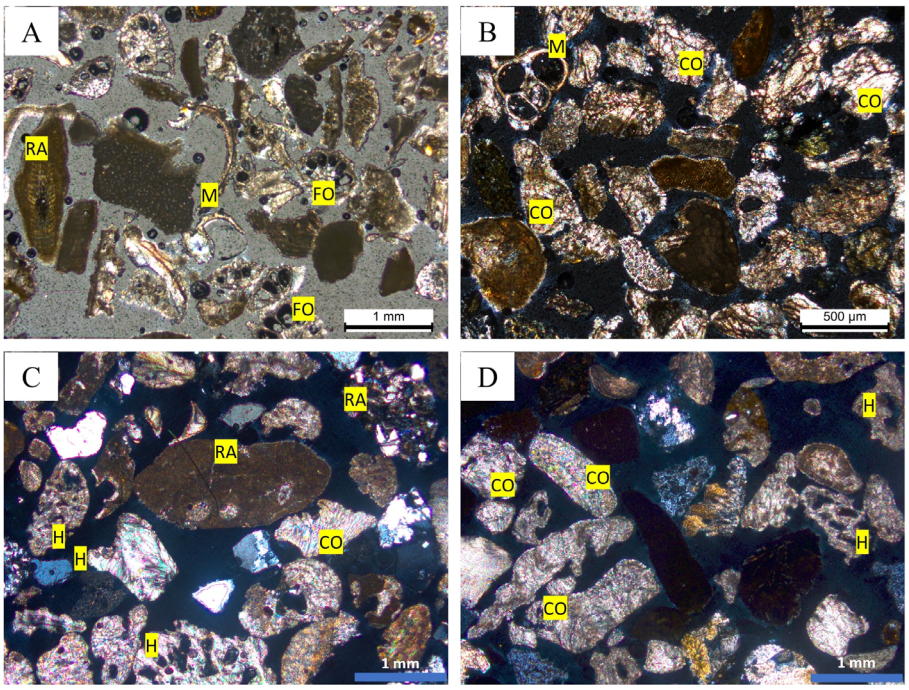

FIGURE 10
Sedimentological characteristics of Biodetrital grainstone. **(A)** Sample from the lower intertidal (<1m water depth) in Badabalu dominated by red algae (RA), molluscs (M) and foraminifera (FO). **(B)** Sample from lower intertidal zone in Burmanallah, constituted by coral fragments (CO) and molluscs. **(C)** Samples from upper intertidal zone of Chotabalu beach, dominated by red algae, *Halimeda* (H) and corals. **(D)** Sample from the upper intertidal zone of Corbyn's Cove, comprised of coral and *Halimeda* fragments.

10.3389/fmars.2024.1481299

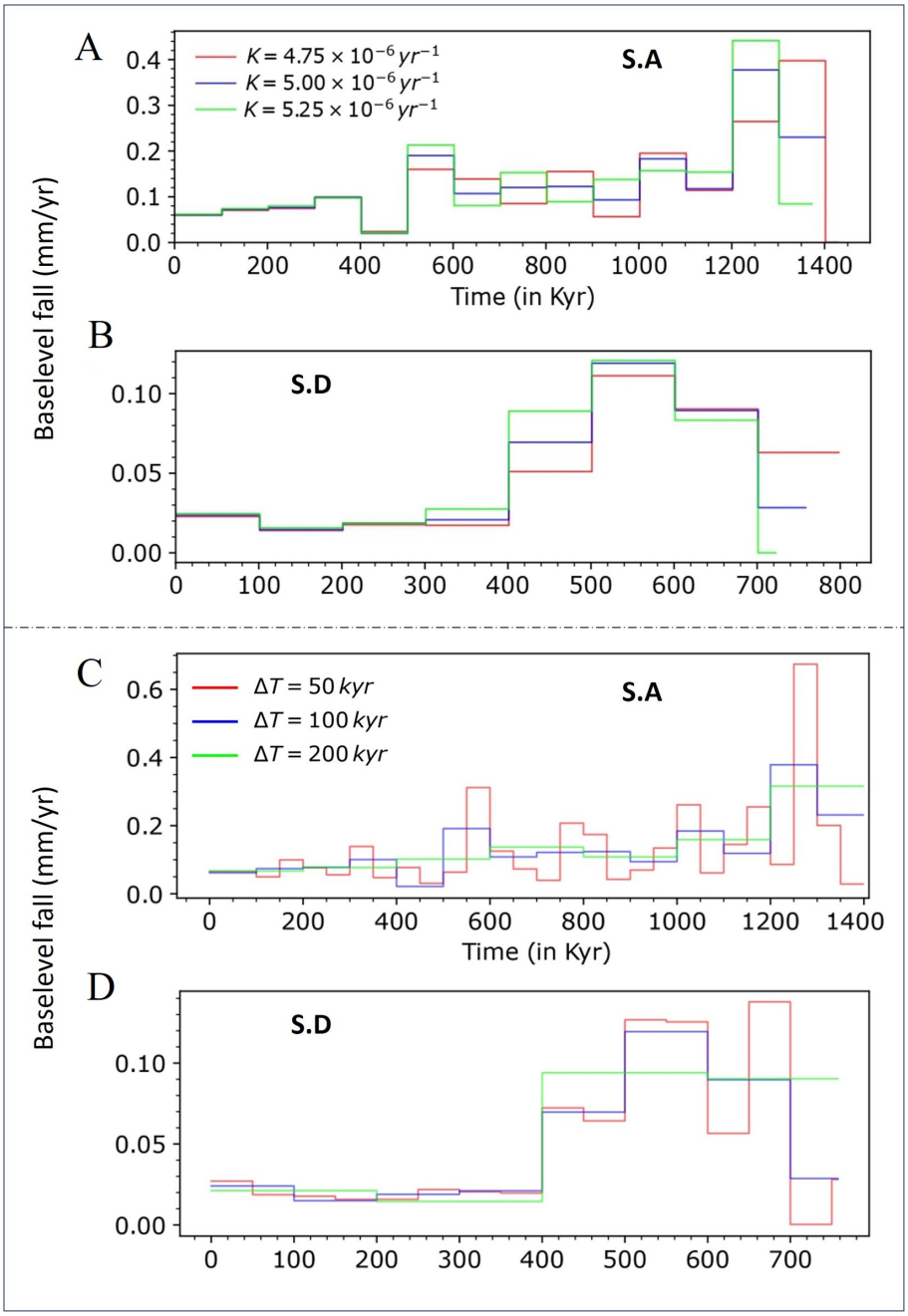

FIGURE 11
The rate of baselevel fall with different values of K (4.75×10^{-6}, 5×10^{-6}, 5.25×10^{-6} yr^{-1}) using similar time interval of Δ= 100 Kyr for **(A)** the south Andaman (S.A) and **(B)** Swaraj Dweep. No significant difference is observed in the magnitude and temporal pattern of the uplift. **(C, D)** Baselevel fall rate for south Andaman (S.A) and Swaraj Dweep (S.D) are obtained for three discrete time intervals: 50 Kyr, 100 Kyr, and 200 Kyr, using a similar K value (K = 5 × 10−6).

similar degree of variability was estimated for Swaraj Dweep, where the rate varies from 0.07 mm/yr (before ~400 Kyr) to a reduced rate of 0.03 mm/yr (from ~400 Kyr to present). Further, we observed that the rate of base-level fall is almost double for south Andaman compared to the Swaraj Dweep. Correspondingly, the magnitude of total base-level change for the last 800 Kyr is almost twice that for south Andaman compared to the Swaraj Dweep (Figure 12).

Despite temporal variations in the uplift rate profiles, the general pattern of temporal fluctuation in island uplift remains unaffected by changes in the erodibility values (Figure 11). Additionally, we also analyzed three distinct time intervals to invert the uplift history keeping same K value. Notably, for smaller time steps (50 Kyr), there was significant variability in the baselevel fall rate. However, the overall trend of baselevel fall rate over time remained similar for varying time steps. The significant variability in baselevel fall rates over older time is attributed to discrepancies between original and synthetic river profiles. Scatter in the older part of the river profiles for the south

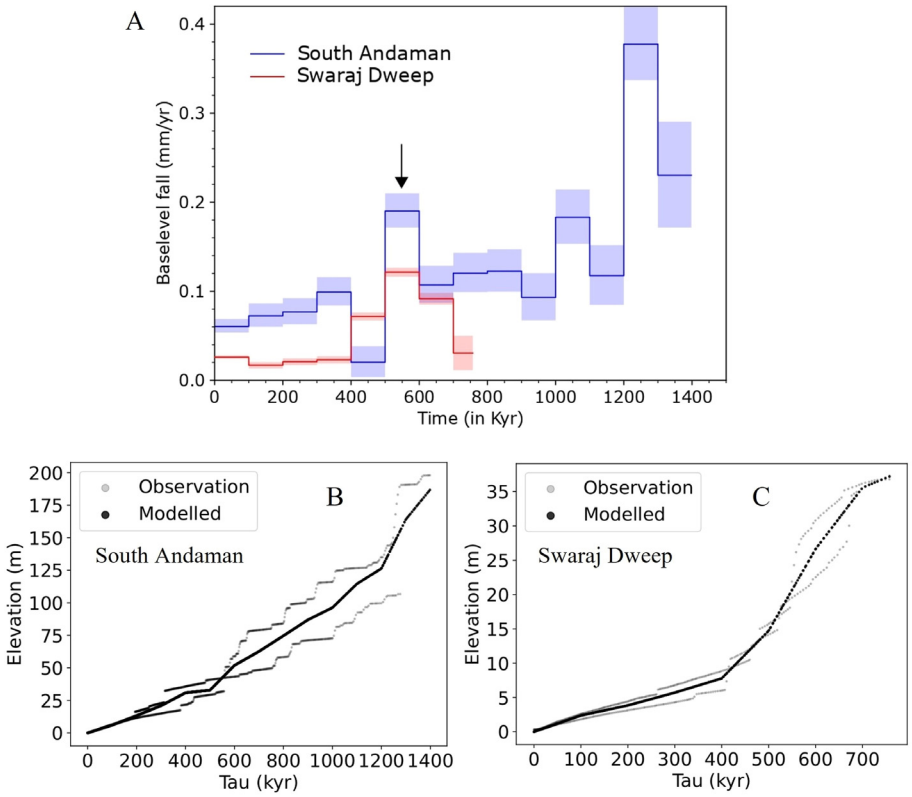

FIGURE 12
Uplift record of the studied Islands. Inversion has been carried out with 0.1 Myr time steps. **(A)** Uplift rates of south Andaman and Swaraj Dweep over the past ~ 1 million years. The uplift rate ranges from 0.06 to 0.36 mm/yr for south Andaman, while for Swaraj Dweep, it varies from 0.02 to 0.1 mm/yr. Shaded bars shows numerical error (1σ) in the model parameter (uplift rate), which is estimated with the help of scatter in the elevation data. **(B)** Original and synthetic river profiles of the south Andaman and **(C)** Swaraj Dweep island. Scatter in the older part of the river profiles for the south Andaman is quite high, resulting in higher uncertainty in the older uplift rates.

Andaman is quite high, resulting higher uncertainty in the older uplift rate (Figure 12B).

Interpretations

Facies interpretation

The modern distribution of facies mapped in this study within the intertidal to shallow marine environments of south Andaman and Swaraj Dweep indicates that corals, algae, molluscs and microfossils (Figure 10) are the main sediment producers along with pebble to cobble sized clasts and the sediments derived from erosion of ophiolites and flysch. The sediments are further re-distributed along the coast due to the local hydrodynamics (influenced by tide, currents, waves and winds).

A dominant rocky shoreline characterizes the eastern margin of south Andaman, whereas the southern and western margins display both the rocky and sandy seashores. The source of the sediments can be distinguished by the color, i.e. erosion of the ophiolites/flysch (dark) or the carbonate sediments (lighter in color). The sand is of a mixed carbonate-siliciclastic origin adjacent to rocky shorelines. The clasts distributed along some of the beaches are formed due to the fragmentation of older mafic rocks, followed by subsequent reshaping and resizing due to local hydrodynamic activity (waves). The silty to muddy siliciclastic sediments brought in by creeks/channels indicate extensive transport from the hinterlands to the shoreline. Carbonate sediments dominate on beaches where no rocky exposures are observed. The sediments are predominantly biogenic, with major components being corals, molluscs, algae and microfossils. Majority of these components are sourced from the modern fringing reef and redistributed along the beach due to local wave and tide-induced currents. The presence of grainstone in the upper intertidal zone indicate moderate to high energy environments and the significant role of wave and tide induced currents in the transportation and redistribution of sediments. In contrast, the beaches of Swaraj Dweep are primarily composed of unconsolidated biodetrital grainstone facies and coralgal boundstone (coral carpets/terraces; Holocene fringing reef). However, in some places, rock layers (mudstone and calcareous siltstone) are observed adjacent to the shoreline. At Radhanagar beach, these rocks exhibit steep dips and are yellow in color. Along Kalapathar beach, the older rocks are greyish in color and contain abundant trace fossils. Most of these rocks belong to the Middle Miocene Inglish and Long Formation (Sharma and Srinivasan, 2007; Bandopadhyay and Carter, 2017).

Beachrock, which is primarily composed of sand to silt-sized carbonate sediments consolidated by carbonate cement, is also observed along the shoreline in Andaman (Chotabalu, Chidiyatapu, Wandoor and Burmanallah). These have formed by the lithification of beach sediments due to constant wave activity. Algal/microbial mats in the rims of the beachrock attest to the cementation due to microbial activity in a high-energy environment (Vousdoukas et al., 2007). A beachrock outcrop from Chidiyatapu, which dates back to 4.4-3.9 ka BP (Rajshekhar and Reddy, 2002), suggests that these facies were formed during the Holocene highstand period (Menon et al., 2023). Additional studies are required to constrain the age (from different locations in Andaman) and origin of these beachrock.

The coralgal boundstone facies occur as terraces/coral carpets, which is a major sea-level dating marker also called 'sea-level indicator' (Rovere et al., 2016a; Khan et al., 2019; Mann et al., 2019; Khanna et al., 2021; Menon et al., 2023). In south Andaman, the dominant exposed coral morphologies are massive to branching predominantly *Porites* sp., including *Porites* microatoll (Figure 4E), while in Swaraj Dweep *Porites* microatoll and platy *Acropora* sp. (Figures 7C, D) are predominant, along with occasional encrusting corals. The presence of these corals within and above the inter-tidal zones in south Andaman and Swaraj Dweep indicates that the sea-level was higher in the recent past, also termed as Holocene Highstand, that has been identified elsewhere in India too (Menon et al., 2023).

Further, the coralgal rudstone are characterized by gravel-sized coral and clastics (pebble to cobble mafic/flysch). The coralgal rudstone facies, with its gravel-sized (large mean size) upturned coral clasts along with volcaniclastic sediments and skewed distribution of grain size could provide evidence of previous overwash deposits (previous storm/cyclonic deposits) (Joyse et al., 2023). The coral clasts are upturned, thus providing evidence of high-energy events transporting the corals from the fringing reef. These deposits are confined to the intertidal zones (limited landward extent) and are dominantly constituted by the beach sediments, further providing evidence of storm deposits (Brill et al., 2020).

Model interpretation

Owing to the active subduction in the region, the studied areas are situated within tectonically active and earthquake prone area (Mishra et al., 2007; Moeremans et al., 2014). Model studies about the earthquake cycle in subduction zones often consider that the upper plate's deformation is entirely elastic and fully restored over multiple cycles of earthquakes (Nicol et al., 2009; Govers et al., 2018). This assumption does not consider any long-lasting vertical movement during the earthquake cycle, especially over thousands of years. However, significant coastal uplift has been documented in several other subduction regions (Such as in Andean margin ~0.1 mm/yr between 122 Kyr and 6 Kyr) over tens of thousands of years that passes through several earthquake cycles (Saillard et al., 2009; Mouslopoulou et al., 2016). So in general, on longer time intervals, uplift tends to dominate the vertical motion of terrestrial fore-arc regions through seismic and aseismic processes (Wilson et al., 2007; Mouslopoulou et al., 2016). Paleo-shoreline indicators, such as multiple tidal notches or uplifted terraces, are observed along the shoreline, however, these indicators may be affected by eustatic changes periodically, potentially masking the underlying tectonic movements (Laborel et al., 1994).

The average uplift rate determined in this study is 0.13 mm/year for south Andaman and 0.05 mm/year for Swaraj Dweep over the course of the past 1.4 and 0.8 million years, respectively (Considering $K = 5\times10^{-6}$ yr^{-1} and $\Delta = 100$ Kyr) (Figures 11, 12A). The eustatic sea-level fluctuated around 120-130 m per 100 Kyr cycles for the last 800 Kyr (Lambeck et al., 2014). However, if we zoom in to examine eustatic changes at smaller time intervals, we find numerous instances where the rate was exceptionally high. For example, if the last 20 Kyr of eustatic rates is considered, the sea-level change rates range from with an average of 6 mm/yr with as high as 40 mm/yr during melt water pulse 1A (MWP-1A; Deschamps et al., 2012), while the average tectonic-driven uplift rate was smaller by a few magnitudes (for e.g. 0.13 mm/yr for south Andaman and 0.05 mm/yr for Swaraj Dweep). As a result, although the exposed coral terraces observed along the coast are formed by a combination of eustatic and tectonic components, the eustatic component clearly outweighs any tectonic component in the formation of younger (millennial year timescale) coral terraces in the current study area.

Discussion

Eustasy and tectonics on Holocene fringing reef

The global mean sea-level is currently rising at a rate of 4.2 mm/yr and this rise has been generally attributed to the melting of ice sheets and the thermal expansion of water (Fox-Kemper et al., 2021; NASA Observatory). It is also essential to note that the sea-level rise/fall rates can vary spatially due to factors such as tectonics, global isostatic adjustments and local factors such as sediment compaction (Rovere et al., 2016b). Thus, the sea-level fluctuations could lead (among other factors that are salinity, temperature, nutrient supply etc.) the shallow marine carbonates to either backstep, downstep, or drown (Sarg, 1988; Schlager, 2005; Brigaud et al., 2014).

In this study, we map the current exposures of the coral terraces/carpets in the intertidal zones along south Andaman and Swaraj Dweep. The corals dated from Swaraj Dweep (Awasthi et al., 2013) has been found to be around 8.7 to 8.4 Kyr BP, while coral terrace from Interview Island has been dated back to ~7.5 Kyr BP and from North Cinque Island corals are dated to be ~700 years to ~1.7 Kyr BP (Figure 1; Rajendran et al., 2008; Kunz et al., 2010). The exposed corals dated from Mayabunder has been found to be around 505 years BP (Figure 1; Yu et al., 2022). Additionally, due to recent Earthquake in 2004, part of Andaman also got uplifted that also has exposed corals that have been dated to be modern in age (Meltzner et al., 2006). To identify which process, i.e. eustasy or

tectonics, is predominant, we further model the uplift rates in south Andaman and Swaraj Dweep, that is an amalgamation of the coseismic deformation along with the interseismic and aseismic surface deformation (Mishra et al., 2021). It is identified that the long-term average uplift rates (0.06 mm/year south Andaman and 0.03mm/year for Swaraj Dweep for the last ~400Kyr) are few tens of times smaller than the eustatic sea-level rise rate. Thus, this study clearly establishes that the eustatic component is the major force driving the formation of Holocene Fringing reefs. The Holocene fringing reef has now down-stepped to the current location of the modern fringing reefs in the subtidal areas of south Andaman and Swaraj Dweep (Figure 13).

Mapping of the Holocene fringing reefs is critical, as they not only provide natural barriers within the intertidal zone but also are going to be the substrate of the future reefs in the context of ongoing eustatic sea-level rise.

Late Quaternary tectonics vs eustasy

Our present study estimates a time-varying long-term tectonic uplift (base-level fall) rate using linear inversion of river profiles from south Andaman and Swaraj Dweep. The results conspicuously show the inherent non-stationary nature of tectonic activity in the forearc region. In both islands, there is a distinct period of tectonic dormancy (low uplift rate) followed by a more active tectonic phase of long-term uplift (nearly doubling of average uplift rates). The average uplift rate of ~0.13 mm/yr for ~1 Myr (south Andaman), and ~0.05 mm/yr for ~800 Kyr (Swaraj Dweep) has been identified. The uplift rate estimated from the inversion model is of the same order of magnitude (toward the lower end) as compared to the long term average uplift rates from other subduction settings such as Cascadia (~0.1mm/yr to ~0.9mm/yr), Makran subduction margin (~0.05 mm/yr to ~1.2mm/yr) and the Andean margin (~0.6mm/yr to ~1mm/yr) (Personius, 1995; Saillard et al., 2009; Pedoja et al., 2014; Normand et al., 2019; Padgett et al., 2019). In this study, older tectonic phases (older than 1 Myr) are a bit ambiguous to interpret owing to the nature of the input elevation data (lesser number of data points with more scatter). However, the rates (0.2-0.4 mm/yr) are within the error limits of the global average rate of base-level change (Pedoja et al., 2014).

These rates could be used as boundary conditions to predict how much uplift has happened of the coastal areas, which could be merged with the information on previous sea level highstands (eustasy driven) to identify the exact elevation of past sea-level highstand carbonates. It is already established that in tectonically active regions the previous highstand deposits are at higher elevations. For example, in the tectonically active region of the Indonesia Archipelago, coral terraces dated to the MIS 5e have been identified, with an average elevation of 34m, indicating the imprint of both eustasy and tectonic uplift (Pedoja et al., 2018). In the Gulf of Aqaba, due to its vicinity to a transform fault, the coastal uplift rate is around 0.15 mm/yr measured from 25 m above MIS 5e deposit (Bosworth et al., 2017). Farther, in the subsiding margin, the past highlands are found at the present-day sea level or below it. For example, in Hawaii, interglacial and older carbonates are reported from the below present-day sea level (Webster et al., 2007). Thus, the coral terraces in south Andaman and Swaraj Dweep can serve as significant sea level indicators for the late Quaternary.

Based on the average uplift rate deduced from this study over the last 400,000 years, the elevations of the MIS 5e, MIS 7, MIS 9, and MIS 11 terraces are expected to be approximately 10 ± 2.5m, 19.2 ± 4.8m, 25.6 ± 6.4m, and 32.8 ± 8.2m on the southern Andaman (with 0.13 mm/yr uplift rate), respectively (Figure 13). At present, no such highstand deposits have been identified in our study area representing MIS 5e or older highstand deposits. This is likely due to erosion caused by prolonged exposure to a tropical climate and/or burial below the extensive vegetation cover.

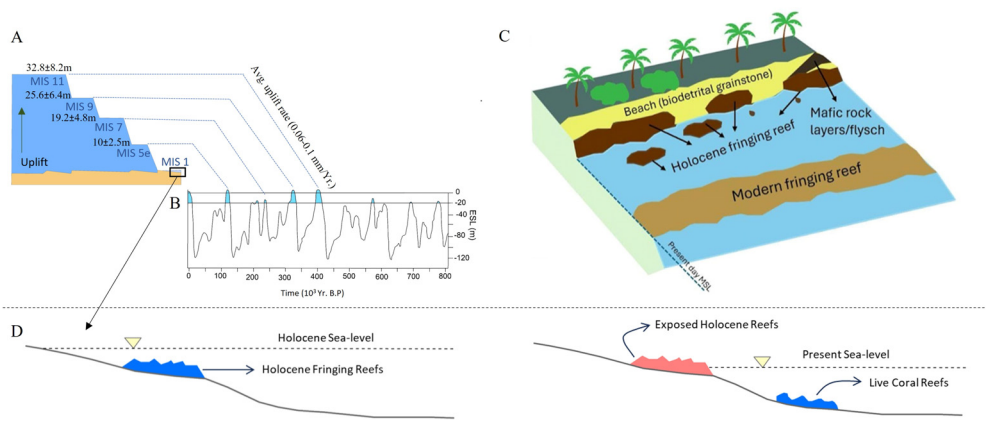

FIGURE 13
(A) Schematic representation illustrating the possible elevations of past highstand carbonate deposits in an uplifting tectonic setting. **(B)** Eustatic sea level fluctuations during Late Quaternary (modified from Waelbroeck et al., 2002; Grant et al., 2014). **(C)** Schematic representation of the modern topography of south Andaman/Swaraj Dweep with the dominant facies. **(D)** Depiction of the response of fringing reef during the Holocene period during elevated sea levels (left) and the illustration of the present-day sea level with live fringing corals and the exposed reefs along the present-day shoreline (right).

Impact of tsunami on fringing reefs

Significant tectonic activity and the establishment of multiple paleotsunami events in the Andaman region indicate the possibility of future earthquake-induced tsunamis. The devastating effects of the 2004 earthquake serve as evidence of the destructive nature of such events, resulting in the damage of low-lying areas along the Andaman coast. These impacts included the uplift of coral terraces (Meltzner et al., 2006; Kayanne et al., 2007), destruction of crop fields and coastal mangroves (as observed in the field) and the displacement of coastal communities (Malik et al., 2019). Given the scenario of rising sea levels, the combination of cyclonic storms and tsunamis in the future could cause even greater damage in the forms of inundation, erosion of the low-lying areas and destruction of the modern fringing reefs.

The Andaman region falls within a subduction zone, making it tectonically active and prone to earthquakes (Mishra et al., 2021), which can potentially trigger tsunamis (Kohl et al., 2005). Numerous studies have focused on gaining insights into past tsunami occurrences by employing sedimentological and geochemical approaches and estimating their ages through accelerator mass spectrometry (AMS) or optically stimulated luminescence (OSL) dating techniques (Jackson et al., 2014; Dura et al.,2015; Malik et al., 2019). In one such study, Malik et al. (2019) collected samples from trenches and cores near the Badabalu beach area and identified a few paleo-tsunami events in the Andaman Islands over the past 8000 years. These events took place in 1881, 1762, and 1679 CE, between 1300 and 1400 CE, as well as in 2000-3000 BCE, 3020-1780 BCE and 5600-5300 BCE (Malik et al., 2019). A separate study Jackson et al. (2014) focused on examining sediment cores collected from a lagoon located on the southeastern coast of Sri Lanka in order to determine the paleo tsunami records during the Holocene period. Organic matter was dated from layers above and below the tsunami deposits to determine their ages. The midpoint ages of these recorded tsunami events have been estimated to 2700, 4200, 4500, 5000, 6200, 6400, and 6600 yr BP (Jackson et al., 2014). It is worth noting that all these tsunami events were triggered by earthquakes occurring along the Andaman-Sumatra subduction zone. These tectonic activities also result in changes in relative sea levels by subsidence or uplift along the coastline (Rovere et al., 2016b). In case of subsidence, the rise in relative sea level could lead to drowning of the reef, as the reefs fail to keep pace with this rise (Schlager, 1981). Subsidence can also occur due to other factors, including the liquefaction of underlying layers due to pressure change (Peltzer et al., 1998; Gahalaut et al., 2008) or viscous deformation in lower crustal or upper mantle area (Hu et al., 2004; Thatcher, 1983). On the other hand, coastal uplift results in a relative sea level drop that exposes parts of the fringing reefs, leading to their demise. Whether rising or falling, sea-level fluctuations significantly impact sediment production and distribution along the shallow shelf and coastal regions (Pomar and Ward, 1995; Kirwan and Megonigal, 2013). Lowland areas are significantly impacted by the rise in sea level, particularly in the subsiding regions located in the southeastern part of the Andaman (Meltzner et al., 2006).

Impact of cyclones on fringing reefs

The Andaman Islands have been prone to a significant number of severe cyclones because of their geographic location. Historical records, such as those found in the "Imperial Gazette of India" (Hunter, 1881), document instances of storms impacting Port Cornvallis (located on Netaji Subhas Chandra Bose Island) in 1792 and 1844, as well as Port Blair in 1864 and 1891. Throughout the twentieth century, the Andaman Islands experienced direct crossings or close passing of strong cyclones in 1911, 1914, 1916, 1921, 1961, 1976, and 1989, which have been recorded by the India Meteorological Department. One particularly noteworthy cyclone occurred in November 1989, when a storm entered the Andaman Sea from the Gulf of Thailand and intensified into a severe cyclonic storm, with wind speeds exceeding 140 km/h (Kumar et al., 2008). This exceptional event resulted in extensive destruction of coastal settlements due to the high wind speeds and generated surge of approximately 2 m, leading to coastal areas being inundated, as observed locally (Kumar et al., 2008). The coralgal rudstone facies mapped in this study within the Brichgunj area, with its gravel-sized (large mean size) upturned coral clasts along with volcaniclastic sediments, provide evidence of previous overwash deposits (previous storm/cyclonic deposits), that should be studied in details to provide better understanding on the processes depositing them. The sediment mostly would have been transported from the fringing reef by the erosion during the cyclonic/storm event.

Recently also, the Andaman Islands have experienced the impact of strong cyclones, including Bulbul in October 2019, Yaas in May 2021, and Jawad in December 2021, all of which caused widespread damage in the region (Tropical weather outlook. India Meteorological Department). These cyclonic events threaten coastal ecosystems, including mangroves and fringing coral communities, due to the flooded water's increased salinity, turbidity, and destructive wave actions (Krauss and Osland, 2020). Thus, with the frequency and intensity of storms expected to increase due to human-induced climate change, substantial variations in sediment supply could have serious repercussions for coastline stability (Abram et al., 2008). Carbonate sediment production in Andaman is determined by the abundance of live fringing reef and the associated reef-dwelling organisms (molluscs, echinoids and other invertebrates); increased incidence of storms could lead to inundation and widespread coral mortality (Baird et al., 2018). In this context, the Holocene Fringing reefs might be useful in preventing coastal erosion owing to stronger wave action caused by storms/cyclones.

Conclusions

This study has mapped and established the presence of Holocene fringing reef along the south Andaman and Swaraj Dweep. The study also tries to identify the underlying processes of reef establishment owing to eustasy and tectonics, as well as also maps the modern sediment distribution in the intertidal zones

within twelve beaches in south Andaman (nine) and Swaraj Dweep (three). The main conclusions are as follows:

1. During Holocene, a fringing reef surrounded the coastal margins of south Andaman and Swaraj Dweep. They are represented by uplifted dead corals (coralgal boundstone) that are massive, branching, and platy in morphology, in addition to microatolls and identified within the intertidal zone. *Porites* and *Acropora* are the main species that represent the exposed corals.
2. The spatial distribution of coastal sediments exhibits a high degree of heterogeneity. The shorelines can be categorized into two - rocky and sandy. The major facies include biodetrital grainstone, coralgal boundstone (coral terraces), beachrock, and coralgal rudstone.
3. The average tectonic movement rates in this study indicates that the uplift rate in Andaman has varied between approximately 0.13 mm/year in south Andaman and 0.05 mm/year in Swaraj Dweep over the course of the past 1.4 and 0.8 million years, respectively. These results provide a relatively long-term (over million-year timescale) tectonic uplift rate for the foreland arc region of the south Andaman, which is an amalgamation of the coseismic deformations along with the interseismic and aseismic surface deformation.
4. The exposed Holocene fringing reef in south Andaman and Swaraj Dweep is attributed predominantly to eustasy. In the wake of accelerated climate change, the global mean sea level(GMSL) rise rate is projected to increase around ~7 mm/yr to ~12 mm/yr in 21st century relative to 1986–2005 GMSL rise rate (Using CMIP5 model in RCP2.5 to RCP 8.5 scenario) (Church et al., 2013), which will aggravate the risks of natural hazards for the population in the low-lying coastal regions, especially in the Andaman Islands.

Data availability statement

The original contributions presented in the study are included in the article/supplementary material. Further inquiries can be directed to the corresponding author.

Author contributions

SKM: Data curation, Formal analysis, Investigation, Methodology, Writing – original draft. SM: Data curation, Formal Analysis, Investigation, Writing – review & editing. RS: Investigation, Methodology, Writing – review & editing. UM: Conceptualization, Investigation, Methodology, Supervision, Writing – review & editing. PK: Conceptualization, Funding acquisition, Investigation, Methodology, Project administration, Resources, Supervision, Writing – review & editing.

Funding

The author(s) declare financial support was received for the research, authorship, and/or publication of this article. This project is funded by IIT Gandhinagar – IP/IITGN/ES/PK/2122/33 and MIS/PMRF/EH/PK/202223/067.

Acknowledgments

The authors would like to thank the Director, IIT Gandhinagar and Director, NGRI for their support. The Ministry of Forests and Environment, Andaman and Nicobar is thanked for all the logistics and technical support during the fieldwork. Continental Labs is acknowledged for the preparation of thin section samples.

Conflict of interest

The authors declare that the research was conducted in the absence of any commercial or financial relationships that could be construed as a potential conflict of interest.

Publisher's note

References

Abram, N. J., Gagan, M. K., Cole, J. E., Hantoro, W. S., and Mudelsee, M. (2008). Recent intensification of tropical climate variability in the Indian Ocean. *Nat. Geosci.* 1, 849–853. doi: 10.1038/ngeo357

Afrizal, R., and Masunaga, T. (2013). Assessment erosion 3D hazard with USLE and surfer tool: a case study of Sumani Watershed in West Sumatra Indonesia. *J. Trop. Soils* 18, 81–92. doi: 10.5400/jts.2013.v18i1.81-92

Allen, R., Carter, A., Najman, Y., Bandopadhyay, P. C., Chapman, H. J., Bickle, M. J., et al. (2008). New constraints on the sedimentation and uplift history of the Andaman-Nicobar accretionary prism, South Andaman Island. *Geological Soc. America*, Special Paper 436. doi: 10.1130/SPE436

Awasthi, N., Ray, J. S., Laskar, A. H., and Yadava, M. G. (2013). Chronology of major terrace forming events in the Andaman Islands during the last 40 Kyr. *J. Geological Soc. India* 82, 59–66. doi: 10.1007/s12594-013-0121-8

Baird, A. H., Álvarez-Noriega, M., Cumbo, V. R., Connolly, S. R., Dornelas, M., and Madin, J. S. (2018). Effects of tropical storms on the demography of reef corals. *Mar. Ecol. Prog. Ser.* 606, 29–38. doi: 10.3354/meps12760

Bandopadhyay, P. C., and Carter, A. (2017). Chapter 11 The Archipelago Group: current understanding. *Geological Society London Memoirs* 47, 153–166. doi: 10.1144/m47.11

Bandyopadhyay, D., van Hinsbergen, D. J., Plunder, A., Bandopadhyay, P. C., Advokaat, E., Chattopadhaya, S., et al. (2020). Andaman ophiolite: an overview. *Andaman Islands Adjoining Offshore: Geology Tectonics Palaeoclimate*, 1–17. doi: 10.1007/978-3-030-39843-9_1

Bosworth, W., Montagna, P., Pons-Branchu, E., Rasul, N., and Taviani, M. (2017). Seismic hazards implications of uplifted pleistocene coral terraces in the gulf of aqaba. *Sci. Rep.* 7 (1), 1–13.

Brigaud, B., Vincent, B., Carpentier, C., Robin, C., Guillocheau, F., Yven, B., et al. (2014). Growth and demise of the Jurassic carbonate platform in the intracratonic Paris Basin (France): interplay of climate change, eustasy and tectonics. *Mar. Petroleum Geology* 53, 3–29. doi: 10.1016/j.marpetgeo.2013.09.008

Brill, D., Seeger, K., Pint, A., Reize, F., Hlaing, K. T., Seeliger, M., et al. (2020). Modern and historical tropical cyclone and tsunami deposits at the coast of Myanmar: Implications for their identification and preservation in the geological record. *Sedimentology* 67, 1431–1459. doi: 10.1111/sed.12586

Buddemeier, R. W., and Hopley, D. (1988). Turn-ons and turn-offs: causes and mechanisms of the initiation and termination of coral reef growth (No. UCRL-98628; CONF-880873-1).

Cabioch, G., Montaggioni, L., Frank, N., Seard, C., Sallé, E., Payri, C., et al. (2008). Successive reef depositional events along the marquesas foreslopes (French polynesia) since 26 ka. *Mar. Geology* 254 (1-2), 18–34.

Chakraborty, A., Ghosh, A. K., and Mazumder, A. (2017). Facies analysis of Pleistocene limestones from Neil West Coast Formation, Neil Island, Ritchie's archipelago of South Andaman, India. *J. Geological Soc. India* 90, 428–436. doi: 10.1007/s12594-017-0736-2

Chakraborty, P. P., and Pal, T. (2001). Anatomy of a forearc submarine fan: upper Eocene—Oligocene andaman flysch group, andaman islands, India. *Gondwana Res.* 4, 477–486. doi: 10.1016/S1342-937X(05)70347-6

Church, J. A., Clark, P. U., Cazenave, A., Gregory, J. M., Jevrejeva, S., Levermann, A., et al. (2013). *Sea level change*. In: *Climate Change 2013: The Physical Science Basis. Contribution of Working Group I to the Fifth Assessment Report of the Intergovernmental Panel on Climate Change*. T. F. Stocker, D. Qin, G.-K. Plattner, M. Tignor, S. K. Allen, J. Boschung, et al. (eds.), Cambridge University Press, Cambridge, United Kingdom and New York, NY, USA.

Clementucci, R., Ballato, P., Siame, L. L., Faccenna, C., Racano, S., Torreti, G., et al. (2023). Transient response to changes in uplift rates in the northern Atlas-Meseta system (Morocco). *Geomorphology* 436, 108765. doi: 10.1016/j.geomorph.2023.108765

Curray, J. R., Moore, D. G., Lawver, L. A., Emmel, F. J., Raitt, R. W., Henry, M., et al. (1979). Tectonics of the Andaman Sea and Burma: convergent margins. *M 29: Geological and Geophysical Investigations of Continental Margins* A109 (1979), 189–198.

Dasgupta, S., Mukhopadhyay, M., Bhattacharya, A., and Jana, T. K. (2003). The geometry of the Burmese- Andaman subducting lithosphere. *J. Seismology* 7, 155–174. doi: 10.1023/A:1023520105384

Davies, P. J., and Hopley, D. (1983). Growth fabrics and growth-rates of Holocene reefs in the Great Barrier-Reef. *BMR J. Aust. Geology Geophysics* 8, 237–251.

Desai, B. G. (2021). Ichnofabric analysis of bathyal chalks: the Miocene Inglis Formation of the Andaman and Nicobar Islands, India. *J. Palaeogeogr.* 10, 494–508. doi: 10.1016/j.jop.2021.11.002

Deschamps, P., Durand, N., Bard, E., Hamelin, B., Camoin, G., Thomas, A. L., et al. (2012). Ice-sheet collapse and sea-level rise at the Bølling warming 14,600 years ago. *Nature* 483, 559–564. doi: 10.1038/nature10902

Dorobek, S. L. (2008). Carbonate-platform facies in volcanic-arc settings: Characteristics and controls on deposition and stratigraphic development. doi: 10.1130/2008.2436(04)

Droxler, A. W., and Jorry, S. J. (2013). Deglacial origin of barrier reefs along low-latitude mixed siliciclastic and carbonate continental shelf edges. *Annu. Rev. Mar. Sci.* 5, 165–190. doi: 10.1146/annurev-marine-121211-172234

Dunham, R. J. (1962). Classification of carbonate rocks according to depositional textures. *Classification of Carbonate Rocks-A Symposium* A038(1962), 108–121.

Dura, T., Cisternas, M., Horton, B. P., Ely, L. L., Nelson, A. R., Wesson, R. L., et al. (2015). Coastal evidence for holocene subduction-zone earthquakes and tsunamis in central chile. *Quaternary Sci. Rev.* 113, 93–111.

Embry, A. F., and Klovan, J. E. (1971). A late Devonian reef tract on northeastern Banks Island, NWT. *Bull. Can. petroleum geology* 19, 730–781. doi: 10.35767/gscpgbull.19.4.730

Flint, J. J. (1974). Stream gradient as a function of order, magnitude, and discharge. *Water Resour. Res.* 10, 969–973. doi: 10.1029/wr010i005p00969

Fox-Kemper, B., Hewitt, H. T., Xiao, C., Aðalgeirsdóttir, G., Drijfhout, S. S., Edwards, T. L., et al. (2021). "Ocean, cryosphere and sea level change," in *Climate Change 2021: The Physical Science Basis. Contribution of Working Group I to the Sixth Assessment Report of the Intergovernmental Panel on Climate Change*. Eds. V. Masson-Delmotte, P. Zhai, A. Pirani, S. L. Connors, C. Péan, S. Berger, et al (Cambridge University Press, Cambridge, United Kingdom and New York, NY, USA), 1211–1362. doi: 10.1017/9781009157896.011

Freeman, L. A., Miller, A. J., Norris, R. D., and Smith, J. E. (2012). Classification of remote Pacific coral reefs by physical oceanographic environment. *J. Geophysical Research: Oceans* 117. doi: 10.1029/2011jc007099

Gahalaut, V. K., Jade, S., Catherine, J. K., Gireesh, R., Ananda, M. B., Kumar, P., et al. (2008). GPS measurements of postseismic deformation in the Andaman-Nicobar region following the giant 2004 Sumatra-Andaman earthquake. *J. Geophysical Research: Solid Earth* 113. doi: 10.1029/2007jb005511

Ghosh, B., Bandyopadhyay, D., and Morishita, T. (2017). Chapter 7 Andaman–Nicobar ophiolites, India: Origin, evolution and emplacement. *Geological Society London Memoirs* 47, 95–110. doi: 10.1144/m47.7

Gibson, R. N., Atkinson, R. J. A., and Gordon, J. D. M. (2007). Coral reefs of the andaman sea–an integrated perspective. *Oceanography Mar. biology: an Annu. Rev.* 45, 173–194.

Goren, L., Fox, M., and Willett, S. D. (2014). Tectonics from fluvial topography using formal linear inversion: Theory and applications to the Inyo Mountains, California. *J. Geophysical Research: Earth Surface* 119, 1651–1681. doi: 10.1002/2014jf003079

Govers, R., Furlong, K. P., Van de Wiel, L., Herman, M. W., and Broerse, T. (2018). The geodetic signature of the earthquake cycle at subduction zones: Model constraints on the deep processes. *Rev. Geophysics* 56, 6–49. doi: 10.1002/2017rg000586

Grant, K. M., Rohling, E. J., Ramsey, C. B., Cheng, H., Edwards, R. L., Florindo, F., et al. (2014). Sea-level variability over five glacial cycles. *Nat. Commun.* 5, 5076. doi: 10.1038/ncomms6076

Greenstein, B. J., and Pandolfi, J. M. (2008). Escaping the heat: range shifts of reef coral taxa in coastal western australia. *Global Change Biol.* 14 (3), 513–528.

Han, J., Gasparini, N. M., Johnson, J. P., and Murphy, B. P. (2014). Modeling the influence of rainfall gradients on discharge, bedrock erodibility, and river profile evolution, with application to the Big Island, Hawai'i. *J. Geophysical Research: Earth Surface* 119, 1418–1440. doi: 10.1002/2013jf002961

Howard, A. D. (1994). A detachment-limited model of drainage basin evolution. *Water Resour. Res.* 30, 2261–2285. doi: 10.1029/94wr00757

Hu, Y., Wang, K., He, J., Klotz, J., and Khazaradze, G. (2004). Three-dimensional viscoelastic finite element model for postseismic deformation of the great 1960 Chile earthquake. *J. Geophysical Research: Solid Earth* 109. doi: 10.1029/2004jb003163

Hunter, W. W. (1881). *The imperial gazetteer of india* (,London: Trubner & Co).

Jackson, K. L., Eberli, G. P., Amelung, F., McFadden, M. A., Moore, A. L., Rankey, E. C., et al. (2014). Holocene Indian Ocean tsunami history in Sri Lanka. *Geology* 42, 859–862. doi: 10.1130/g35796.1

Joyse, K. M., Khan, N. S., Moyer, R. P., Radabaugh, K. R., Hong, I., Chappel, A. R., et al. (2023). The characteristics and preservation potential of Hurricane Irma's overwash deposit in southern Florida, USA. *Mar. Geology* 461, 107077. doi: 10.1016/j.margeo.2023.107077

Kayanne, H., Ikeda, Y., Echigo, T., Shishikura, M., Kamataki, T., Satake, K., et al. (2007). Coseismic and postseismic creep in the Andaman Islands associated with the 2004 Sumatra-Andaman earthquake. *Geophysical Res. Lett.* 34. doi: 10.1029/2006gl028200

Kennedy, D. M., and Woodroffe, C. D. (2002). Fringing reef growth and morphology: a review. *Earth-Science Rev.* 57, 255–277. doi: 10.1016/s0012-8252(01)00077-0

Khan, N. S., Horton, B. P., Engelhart, S., Rovere, A., Vacchi, M., Ashe, E. L., et al. (2019). Inception of a global atlas of sea levels since the Last Glacial Maximum. *Quaternary Sci. Rev.* 220, 359–371. doi: 10.1016/j.quascirev.2019.07.016

Khanna, P., Droxler, A. W., Nittrouer, J. A., Tunnell, J. J.W., and Shirley, T. C. (2017). Coralgal reef morphology records punctuated sea-level rise during the last deglaciation. *Nat. Commun.* 8, 1046. doi: 10.1038/s41467-017-00966-x

Khanna, P., Petrovic, A., Ramdani, A. I., Homewood, P., Mettraux, M., and Vahrenkamp, V. (2021). Mid-Holocene to present circum-Arabian sea level database: Investigating future coastal ocean inundation risk along the Arabian plate shorelines. *Quaternary Sci. Rev.* 261, 106959. doi: 10.1016/j.quascirev.2021.106959

Khanna, P., Pyrcz, M., Droxler, A. W., Hopson, H. H., Harris, P. M. M., and Lehrmann, D. J. (2020). Implications for controls on Upper Cambrian microbial build-ups across multiple-scales, Mason County, Central Texas, USA. *Mar. Petroleum Geology* 121, 104590. doi: 10.1016/j.marpetgeo.2020.104590

Kirby, E., and Whipple, K. X. (2012). Expression of active tectonics in erosional landscapes. *J. Struct. geology* 44, 54–75. doi: 10.1016/j.jsg.2012.07.009

Kirwan, M. L., and Megonigal, J. P. (2013). Tidal wetland stability in the face of human impacts and sea-level rise. *Nature* 504, 53–60. doi: 10.1038/nature12856

Kohl, P. A., O'Rourke, A. P., Schmidman, D. L., Dopkin, W. A., and Birnbaum, M. L. (2005). The Sumatra-Andaman earthquake and tsunami of 2004: the hazards, events, and damage. *Prehospital Disaster Med.* 20, 355–363. doi: 10.1017/s1049023x00002880

Krauss, K. W., and Osland, M. J. (2020). Tropical cyclones and the organization of mangrove forests: a review. *Ann. Bot.* 125, 213–234. doi: 10.1093/aob/mcz161

Kumar, V. S., Babu, V. R., Babu, M. T., Dhinakaran, G., and Rajamanickam, G. V. (2008). Assessment of storm surge disaster potential for the Andaman Islands. *J. Coast. Res.* 24), 171–177. doi: 10.2112/05-0506.1

Kunz, A., Frechen, M., Ramesh, R., and Urban, B. (2010). Revealing the coastal event-history of the Andaman Islands (Bay of Bengal) during the Holocene using radiocarbon and OSL dating. *Int. J. Earth Sci.* 99, 1741–1761. doi: 10.1007/s00531-009-0507-4

Laborel, J., Morhange, C., Lafont, R., Le Campion, J., Laborel-Deguen, F., and Sartoretto, S. (1994). Biological evidence of sea-level rise during the last 4500 years on the rocky coasts of continental southwestern France and Corsica. *Mar. Geology* 120, 203–223. doi: 10.1016/0025-3227(94)90059-0

Lambeck, K., Esat, T. M., and Potter, E. K. (2002). Links between climate and sea levels for the past three million years. *Nature* 419, 199–206. doi: 10.1038/nature01089

Lambeck, K., Rouby, H., Purcell, A., Sun, Y., and Sambridge, M. (2014). Sea level and global ice volumes from the Last Glacial Maximum to the Holocene. *Proc. Natl. Acad. Sci.* 111, 15296–15303. doi: 10.1073/pnas.1411762111

Lenihan, H. S., Hench, J. L., Holbrook, S. J., Schmitt, R. J., and Potoski, M. (2015). Hydrodynamics influence coral performance through simultaneous direct and indirect effects. *Ecology* 96, 1540–1549. doi: 10.1890/14-1115.1

Lindsay, J. B. (2016). Whitebox GAT: A case study in geomorphometric analysis. *Comput. Geosciences* 95, 75–84. doi: 10.1016/j.cageo.2016.07.003

Ma, Z., Zhang, H., Wang, Y., Tao, Y., and Li, X. (2020). Inversion of Dadu River bedrock channels for the late Cenozoic uplift history of the eastern Tibetan Plateau. *Geophysical Res. Lett.* 47, e2019GL086882. doi: 10.1029/2019gl086882

Magnan, A. K., Garschagen, M., Gattuso, J. P., Hay, J. E., Hilmi, N., Holland, E. A., et al. (2019). Cross-Chapter Box 9: Integrative Cross-Chapter Box on Low-Lying Islands and Coasts. In: *IPCC Special Report on the Ocean and Cryosphere in a Changing Climate*. doi: 10.1017/9781009157964

Malik, J. N., Johnson, F. C., Khan, A., Sahoo, S., Irshad, R., Paul, D., et al. (2019). Tsunami records of the last 8000 years in the Andaman Island, India, from mega and large earthquakes: Insights on recurrence interval. *Sci. Rep.* 9, 18463. doi: 10.1038/s41598-019-54750-6

Mann, T., Bender, M., Lorscheid, T., Stocchi, P., Vacchi, M., Switzer, A. D., et al. (2019). Holocene sea levels in Southeast Asia, Maldives, India and Sri Lanka: The SEAMIS database. *Quaternary Sci. Rev.* 219, 112–125. doi: 10.1016/j.quascirev.2019.07.007

Meltzner, A. J., Sieh, K., Abrams, M., Agnew, D. C., Hudnut, K. W., Avouac, J. P., et al. (2006). Uplift and subsidence associated with the great Aceh-Andaman earthquake of 2004. *J. geophysical Res.* 111. doi: 10.1029/2005jb003891

Meltzner, A. J., Sieh, K., Chiang, H. W., Shen, C. C., Suwargadi, B. W., Natawidjaja, D. H., et al. (2010). Coral evidence for earthquake recurrence and an AD 1390–1455 cluster at the south end of the 2004 Aceh–Andaman rupture. *J. Geophysical Research: Solid Earth* 115. doi: 10.1029/2010jb007499

Menier, D., Pierson, B., Chalabi, A., Ting, K. K., and Pubellier, M. (2014). Morphological indicators of structural control, relative sea-level fluctuations and platform drowning on present-day and Miocene carbonate platforms. *Mar. Petroleum Geology* 58, 776–788. doi: 10.1016/j.marpetgeo.2014.01.016

Menon, S., Khanna, P., and Banerjee, S. (2023). Circum-Indian Holocene sea-level database: A repository of distinct relative sea-level plots across the Indian Peninsula. *J. Palaeogeogr.* 13, 1–17. doi: 10.1016/j.jop.2023.10.003

Menon, S., Khanna, P., Misra, S. K., and Jorry, S. J. (2024). Decadal timescale evolution of coral islands: insights from lakshadweep archipelago. *Front. Mar. Sci.* 11, 1431655.

Mishra, M., Abhishek,, Yadav, R. B. S., and Sandhu, M. (2021). Probabilistic assessment of earthquake hazard in the Andaman–Nicobar–Sumatra region. *Natural Hazards* 105, 313–338. doi: 10.1007/s11069-020-04311-2

Mishra, O. P., Kayal, J. R., Chakrabortty, G. K., Singh, O. P., and Ghosh, D. (2007). Aftershock investigation in the Andaman–Nicobar Islands of India and its seismotectonic implications. *Bull. Seismological Soc. America* 97, S71–S85. doi: 10.1785/0120050629

Moeremans, R., Singh, S. C., Mukti, M., McArdle, J., and Johansen, K. (2014). Seismic images of structural variations along the deformation front of the Andaman–Sumatra subduction zone: implications for rupture propagation and tsunamigenesis. *Earth Planetary Sci. Lett.* 386, 75–85. doi: 10.1016/j.epsl.2013.11.003

Montaggioni, L. F. (2005). History of Indo-Pacific coral reef systems since the last glaciation: development patterns and controlling factors. *Earth-Science Rev.* 71, 1–75. doi: 10.1016/j.earscirev.2005.01.002

Montgomery, D. R., and Gran, K. B. (2001). Downstream variations in the width of bedrock channels. *Water Resour. Res.* 37, 1841–1846. doi: 10.1029/2000wr900393

Morales, B., Lizama, E., Somos-Valenzuela, M., Rivera, D., and Ningshen, C. (2023). Earthquake-induced landslides coupled to fluvial incision in Andean Patagonia: Inferring their effects on landscape at geological time scales. *Geomorphology* 434, 108731. doi: 10.1016/j.geomorph.2023.108731

Mouslopoulou, V., Oncken, O., Hainzl, S., and Nicol, A. (2016). Uplift rate transients at subduction margins due to earthquake clustering. *Tectonics* 35, 2370–2384. doi: 10.1002/2016tc004248

Neumann, A. C. (1985). Reef response to sea level rise: Keep-up, catch-up or give-up. *In Proc. Fifth Intern. Coral Reef Congr. Tahiti* 3, 105–110. doi: 10.1371/journal.pone.0118571

Neumann, B., Vafeidis, A. T., Zimmermann, J., and Nicholls, R. J. (2015). Future coastal population growth and exposure to sea-level rise and coastal flooding-a global assessment. *PloS One* 10, e0118571.

Nicol, A., Walsh, J., Mouslopoulou, V., and Villamor, P. (2009). Earthquake histories and Holocene acceleration of fault displacement rates. *Geology* 37, 911–914. doi: 10.1130/g25765a.1

Normand, R., Simpson, G., Herman, F., Biswas, R. H., Bahroudi, A., and Schneider, B. (2019). Dating and morphostratigraphy of uplifted marine terraces in the Makran subduction zone (Iran). *Earth Surface Dynamics* 7, 321–344. doi: 10.5194/esurf-7-321-2019

Padgett, J. S., Kelsey, H. M., and Lamphear, D. (2019). Upper-plate deformation of Late Pleistocene marine terraces in the Trinidad, California, coastal area, southern Cascadia subduction zone. *Geosphere* 15, 1323–1341. doi: 10.1130/ges02032.1

Pedersen, V. K., Braun, J., and Huismans, R. S. (2018). Eocene to mid-Pliocene landscape evolution in Scandinavia inferred from offshore sediment volumes and pre-glacial topography using inverse modelling. *Geomorphology* 303, 467–485. doi: 10.1016/j.geomorph.2017.11.025

Pedoja, K., Husson, L., Bezos, A., Pastier, A., Imran, A. M., Arias-Ruiz, C., et al. (2018). On the long-lasting sequences of coral reef terraces from SE Sulawesi (Indonesia): Distribution, formation, and global significance. *Quaternary Sci. Rev.* 188, 37–57. doi: 10.1016/j.quascirev.2018.03.033

Pedoja, K., Husson, L., Johnson, M. E., Melnick, D., Witt, C., Pochat, S., et al. (2014). Coastal staircase sequences reflecting sea-level oscillations and tectonic uplift during the Quaternary and Neogene. *Earth-Science Rev.* 132, 13–38. doi: 10.1016/j.earscirev.2014.01.007

Peltzer, G., Rosen, P., Rogez, F., and Hudnut, K. (1998). Poroelastic rebound along the Landers 1992 earthquake surface rupture. *J. Geophysical Research: Solid Earth* 103, 30131–30145. doi: 10.1029/98jb02302

Perry, C. T. (2003). Coral reefs in a high-latitude, siliciclastic barrier island setting: reef framework and sediment production at Inhaca Island, southern Mozambique. *Coral Reefs* 22, 485–497. doi: 10.1007/s00338-003-0339-9

Personius, S. F. (1995). Late Quaternary stream incision and uplift in the forearc of the Cascadia subduction zone, western Oregon. *J. Geophysical Research: Solid Earth* 100, 20193–20210. doi: 10.1029/95jb01684

Petrovic, A., Fuentes, M. A., Putri, I., Yahaya, L. N., Khanna, P., Purkis, S. J., et al. (2022). Holocene sediment distribution in the Al Wajh platform lagoon (northern Red Sea, Saudi Arabia), a modern analogue for large rift basin carbonate platforms. *Sedimentology* 69, 1365–1398. doi: 10.1111/sed.12955

Pomar, L., and Ward, W. C. (1995). "Sea-level changes, carbonate production and platform architecture: the Llucmajor Platform, Mallorca, Spain," in *Sequence stratigraphy and depositional response to eustatic, tectonic and climatic forcing* (Springer Netherlands, Dordrecht), 87–112.

Pritchard, D., Roberts, G. G., White, N. J., and Richardson, C. N. (2009). Uplift histories from river profiles. *Geophysical Res. Lett.* 36. doi: 10.1029/2009gl040928

Rajendran, K., Rajendran, C. P., Earnest, A., Prasad, G. R., Dutta, K., Ray, D. K., et al. (2008). Age estimates of coastal terraces in the Andaman and Nicobar Islands and their tectonic implications. *Tectonophysics* 455, 53–60. doi: 10.1016/j.tecto.2008.05.004

Rajshekhar, C., and Reddy, P. P. (2002). Ecology of beachrock fauna of the south Andaman Island, Bay of Bengal. *Curr. Sci.* 82, 881–885.

Ray, K. K., Sengupta, S., and Van Den Hul, H. J. (1988). Chemical characters of volcanic rocks from Andaman ophiolite, India. *J. Geological Soc.* 145, 393–400. doi: 10.1144/gsjgs.145.3.0393

Rodolfo, K. S. (1969). Bathymetry and marine geology of the andaman basin, and tectonic implications for southeast asia. *Geological Soc. America Bull.* 80 (7), 1203–1230.

Rovere, A., Raymo, M. E., Vacchi, M., Lorscheid, T., Stocchi, P., Gomez-Pujol, L., et al. (2016a). The analysis of Last Interglacial (MIS 5e) relative sea-level indicators: Reconstructing sea-level in a warmer world. *Earth-Science Rev.* 159, 404–427. doi: 10.1016/j.earscirev.2016.06.006

Rovere, A., Stocchi, P., and Vacchi, M. (2016b). Eustatic and relative sea level changes. *Curr. Climate Change Rep.* 2, 221–231. doi: 10.1007/s40641-016-0045-7

Saillard, M., Hall, S. R., Audin, L., Farber, D. L., Hérail, G., Martinod, J., et al. (2009). Non- steady long-term uplift rates and Pleistocene marine terrace development along the Andean margin of Chile (31S) inferred from 10Be dating. *Earth Planetary Sci. Lett.* 277, 50–63. doi: 10.1016/j.epsl.2008.09.039

Sarg, J. F. (1988). Carbonate sequence stratigraphy. *Sea-Level Changes- An Integrated Approach, SEPM Special Publication No. 42, Copyright 1988, The Society of Economic Paleontologists and Mineralogists.*

Schlager, W. (1981). The paradox of drowned reefs and carbonate platforms. *Geological Soc. America Bull.* 92, 197–211. doi: 10.1130/0016-7606(1981)92<197:tpodra>2.0.co;2

Schlager, W. (2005). Carbonate sedimentology and sequence stratigraphy (No. 8). *SEPM Soc. Sed Geology*. doi: 10.2110/csp.05.08

Schwanghart, W., and Scherler, D. (2014). TopoToolbox 2–MATLAB-based software for topographic analysis and modeling in Earth surface sciences. *Earth Surface Dynamics* 2, 1–7. doi: 10.5194/esurf-2-1-2014

Sharma, V., and Srinivasan, M. S. (2007). *Geology of Andaman-Nicobar: The Neogene* (New Delhi: Capital Publishing Company). 1-164 pp.

Sonam,, Sahoo, R., Singh, R. N., and Jain, V. (2021). Temporal profiling of uplift rate along an active fault using river long profile in the Kuchchh region, Western India. *Quaternary Int.* 585, 85–98. doi: 10.1016/j.quaint.2020.11.022

Steers, J. A., Stoddart, D. R., Jones, O. A., and Endean, R. (1977). The origin of fringing reefs, barrier reefs and atolls. *Biol. Geology Coral Reefs. Geology* 2, 21–57.

Stucky de Quay, G., Kite, E. S., and Mayer, D. P. (2019). Prolonged fluvial activity from channel-fan systems on Mars. *J. Geophysical Research: Planets* 124, 3119–3139. doi: 10.1029/2019JE006167

Su, Q., Wang, X., Yuan, D., Zhang, H., Lu, H., and Xie, H. (2022). Secondary faulting plays a key role in regulating the Cenozoic crustal deformation in the northeastern Qinghai-Tibet Plateau. *Terra Nova* 34, 231–243. doi: 10.1111/ter.12583

Thatcher, W. (1983). Nonlinear strain buildup and the earthquake cycle on the San Andreas fault. *J. Geophysical Research: Solid Earth* 88, 5893–5902. doi: 10.1029/jb088ib07p05893

Tropical weather outlook. India Meteorological Department. Available online at: https://mausam.imd.gov.in/responsive/cyclone_bulletin_archive.php?id=1 (Accessed July 20, 2023).

Vousdoukas, M., Velegrakis, A., and Plomaritis, T. (2007). Beachrock occurrence, characteristics, formation mechanisms and impacts. *Earth-Science Rev.* 85, 23–46. doi: 10.1016/j.earscirev.2007.07.002

Waelbroeck, C., Labeyrie, L., Michel, E., Duplessy, J. C., Mcmanus, J. F., Lambeck, K., et al. (2002). Sea-level and deep water temperature changes derived from benthic foraminifera isotopic records. *Quaternary Sci. Rev.* 21 (1-3), 295–305.

Wafar, M. V. M (1986). Corals and coral reefs of India. *Proceedings of the Indian Academy of Sciences* (Animal Science/Plant Science), 19–43.

Wall, M., Schmidt, G. M., Janjang, P., Khokiattiwong, S., and Richter, C. (2012). Differential impact of monsoon and large amplitude internal waves on coral reef development in the Andaman Sea. *PloS One* 7, e50207. doi: 10.1371/journal.pone.0050207

Webster, J. M., Wallace, L. M., Clague, D. A., and Braga, J. C. (2007). Numerical modeling of the growth and drowning of Hawaiian coral reefs during the last two glacial cycles (0–250 Kyr). *Geochemistry Geophysics Geosystems* 8. doi: 10.1029/2006gc001415

Whipple, K. X., and Tucker, G. E. (1999). Dynamics of the stream-power river incision model: Implications for height limits of mountain ranges, landscape response timescales, and research needs. *J. Geophysical Research: Solid Earth* 104, 17661–17674. doi: 10.1029/1999jb900120

Wilson, K., Berryman, K., Cochran, U., and Little, T. (2007). Holocene coastal evolution and uplift mechanisms of the northeastern Raukumara Peninsula, North Island, New Zealand. *Quaternary Sci. Rev.* 26, 1106–1128. doi: 10.1016/j.quascirev.2007.01.005

Wohl, E. (2020). Rivers in the anthropocene: the US perspective. *Geomorphology* 366, 106600. doi: 10.1016/j.geomorph.2018.12.001

Woodroffe, C. D., and Webster, J. M. (2014). Coral reefs and sea-level change. *Mar. Geology* 352, 248–267. doi: 10.1016/j.margeo.2013.12.006

Yamano, H., Abe, O., Matsumoto, E., Kayanne, H., Yonekura, N., and Blanchon, P. (2003). Influence of wave energy on Holocene coral reef development: an example from Ishigaki Island, Ryukyu Islands, Japan. *Sedimentary Geology* 159, 27–41. doi: 10.1016/s0037-0738(03)00093-9

Yanites, B. J., Becker, J. K., Madritsch, H., Schnellmann, M., and Ehlers, T. A. (2017). Lithologic effects on landscape response to base level changes: A modeling study in the context of the eastern Jura Mountains, Switzerland. *J. Geophysical Research: Earth Surface* 122, 2196–2222. doi: 10.1002/2016jf004101

Yu, Y., Hathorne, E., Siebert, C., Felis, T., Rajendran, C. P., and Frank, M. (2022). Monthly resolved coral barium isotopes record increased riverine inputs during the south asian summer monsoon. *Geochimica Cosmochimica Acta* 329, 152–167.